ACS OMEGA

Open Access

http://pubs.acs.org/journal/acsodf

Article

Identification of Novel, Potent, and Selective Compounds against Malaria Using Glideosomal-Associated Protein 50 as a Drug Target

Prakhar Agrawal,* Surekha Kumari, Asif Mohmmed, Pawan Malhotra,* Upendra Sharma, and Dinkar Sahal

Cite This: *ACS Omega* 2023, 8, 38506−38523

Read Online

ACCESS | Metrics & More | Article Recommendations | Supporting Information

ABSTRACT: Phylum apicomplexan consists of parasites, such as *Plasmodium* and *Toxoplasma*. These obligate intracellular parasites enter host cells *via* an energy-dependent process using specialized machinery, called the glideosome. In the present study, we used *Plasmodium falciparum* GAP50, a glideosome-associated protein, as a target to screen 951 different compounds from diverse chemical libraries. Using different screening methods, eight compounds (Hayatinine, Curine, MMV689758 (Bedaquiline), MMV1634402 (Brilacidin), and MMV688271, MMV782353, MMV642550, and USINB4-124-8) were identified, which showed promising binding affinity (KD < 75 μM), along with submicromolar range antiparasitic efficacy and selectivity index > 100 fold for malaria parasite. These eight compounds were effective against Chloroquine-resistant *Pf*INDO and Artemisinin-resistant *Pf*Cam3.1^{R359T} strains. Studies on the effect of these compounds at asexual blood stages showed that these eight compounds act differently at different developmental stages, indicating the binding of these compounds to other *Plasmodium* proteins, in addition to *Pf*GAP50. We further studied the effects of compounds (Bedaquiline and USINB4-124-8) in an *in vivo Plasmodium berghei* mouse model of malaria. Importantly, the oral delivery of Bedaquiline (50 mg/kg b. wt.) showed substantial suppression of parasitemia, and three out of seven mice were cured of the infection. Thus, our study provides new scaffolds for the development of antimalarials that can act at multiple *Plasmodium* lifecycle stages.

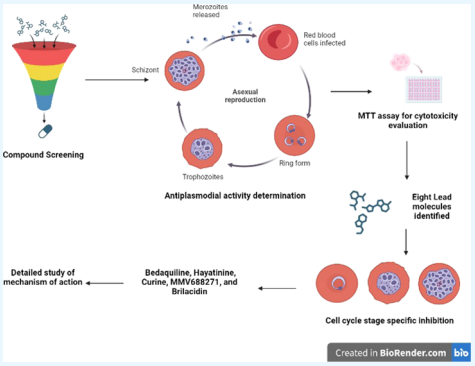

INTRODUCTION

Malaria continues to be a deadly illness in the world, mainly in Africa, Asia, and South America. With the rapid emergence of drug-resistant parasite strains, there is a need to identify new antimalarial agents that can act on novel targets. Apicomplexans possess a unique, conserved, and essential mechanism of motility and host cell invasion, and these molecular mechanisms and their components are promising chemotherapeutic targets.[1] Despite differences in cell shapes and types associated with distinct invasive stages of *Plasmodium* spp. (*e.g.*, erythrocytes by merozoites, mosquito salivary glands by ookinetes, and hepatocytes by sporozoites), each invasive stage maintains similar overall morphology along with associated organelles, and many proteins associated with motility remain conserved.[2−4]

Plasmodium merozoite invasion of RBCs is a critical and multistep process[4] involving the attachment of merozoites to the RBC surface, reorientation of merozoites, tight junction formation, and subsequent gliding of merozoites into RBCs. Several merozoite surfaces and secretory proteins, such as MSP-1,[5] MSP-2,[6] AMA-1,[7] Rh-5,[8] EBA-175,[9] and Enolase,[10] are involved in the first three steps of invasion.[11] The gliding of merozoites into RBCs is driven by an actin−myosin motor structure referred to as the "glideosome" that is housed in the pellicle of the zoite and is linked both to the inner-membrane complex (IMC) and parasite plasma membrane. Glideosome allows parasite adhesion molecules on the surface to connect to actin filaments in the pellicle, resulting in progressive movement by the force of the myosin motor.[12,13] To date, a complete repertoire of IMC and glideosome proteins has not been reported because of the difficulty in separating IMC and glideosome proteins from other membrane proteins. Recently, a collection of 300 proteins was identified as IMC and IMC-associated proteins in a rodent malaria parasite *Plasmodium yoelii*, by Turbo-labeling and quantitative MS/MS.[14] Some of the characterized IMC proteins include glideosome-associated protein 45 (GAP45), GAP40, GAP50, Myosin A tail interacting protein (MTIP), MyoA, ECL1, GAPs with multiple membrane spanning regions (GAPM1, GAPM2, GAPM3), ISP1, ISP3, PhiL1, and several alveolin proteins.[15−18] Many of these proteins, such as myosin A heavy chain (MyoA), the myosin light chain TgMLCI (or *Pf*MTIP), and two glideosome-

Received: July 23, 2023
Accepted: September 1, 2023
Published: October 6, 2023

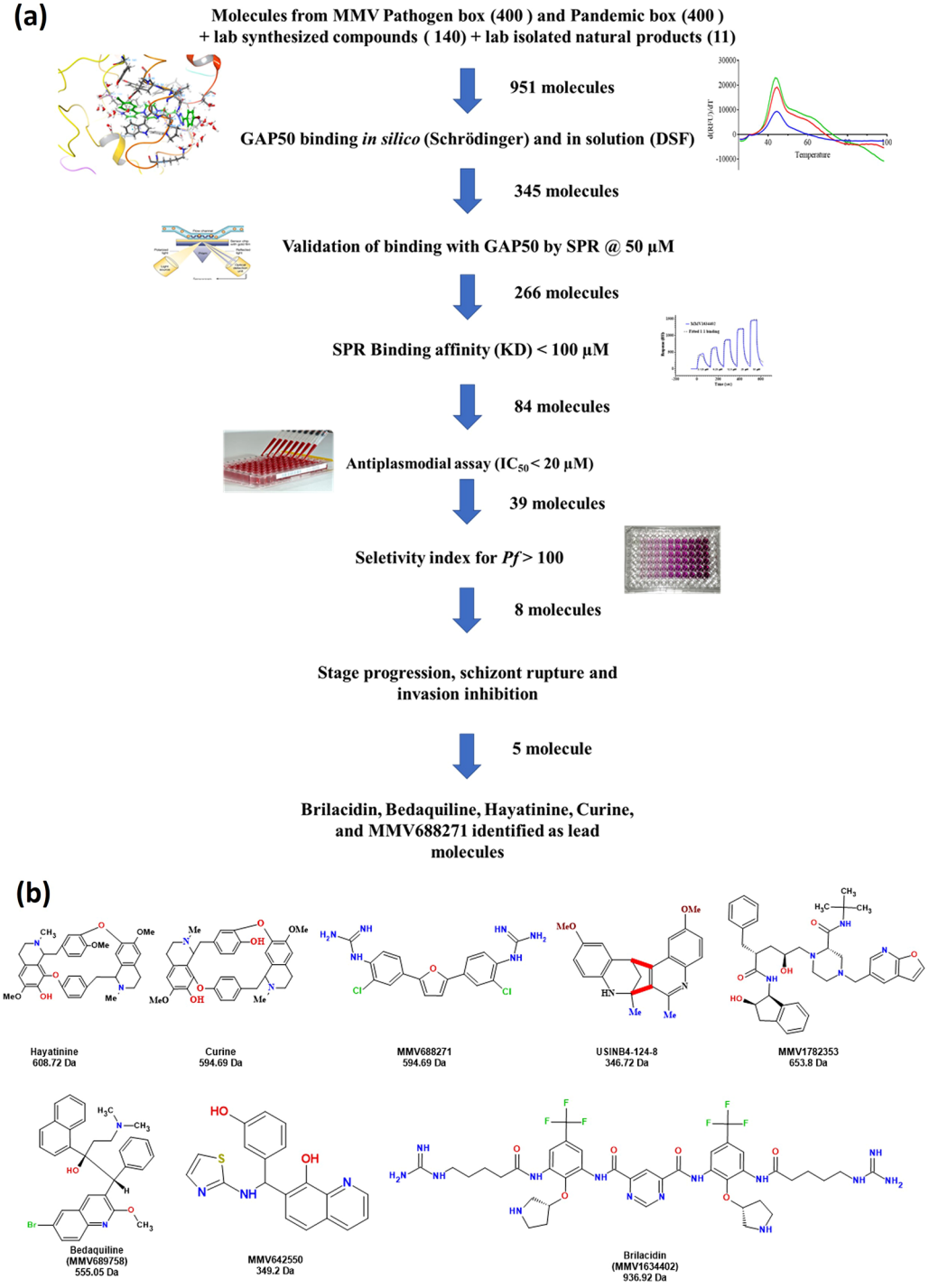

Figure 1. Selection of molecules at successive stages of molecular, cellular, and *in vivo* animal screening. (a) Flowchart showing the pool of 951 molecules coming from diverse sources and the progressively decreasing numbers of shortlisted molecules at successive stages of different kinds of screens. (b) Structure of the eight *Pf* GAP50 binder hit molecules with antiplasmodial $IC_{50} < 3\ \mu M$ and selectivity indices ≥100. Hayatinine and Curine were isolated from *C. pareira*, USINB4-124-8 is an azepino quinoline, and the remaining molecules that have come from the MMV pathogen and pandemic boxes are of diverse chemical natures including piperazine carboxamide (MMV1782353), pyrimidine dicarboxamide (Brilacidin), Benzimidazole (MMV642550), quinoline (Bedaquiline), and 2,5-diphenyl furan (MMV688271).

associated proteins, GAP45 and GAP50, are also part of the glideosome machinery.[13,19] It has been suggested that the motor complex is assembled as a soluble precomplex of MyoA-MLCI-GAP45 proteins in the cytosol before being anchored to the membrane by GAP50.[20]

The involvement of gliding machinery in the invasion of both sexual and asexual stages of *Plasmodium* and the absence of analogous proteins in humans make the components of gliding machinery ideal drug targets for antimalarial drug discovery.[21−24] Among the different proteins of the glideosomal complex,[20,25−29] here we target the glideosome-associated protein 50, an essential protein in all apicomplexan parasites, including *Plasmodium, Toxoplasma*, and *Cryptosporidium*. GAP50, highly conserved in Apicomplexans,[2] plays a pivotal

https://doi.org/10.1021/acsomega.3c05323
ACS Omega 2023, 8, 38506−38523

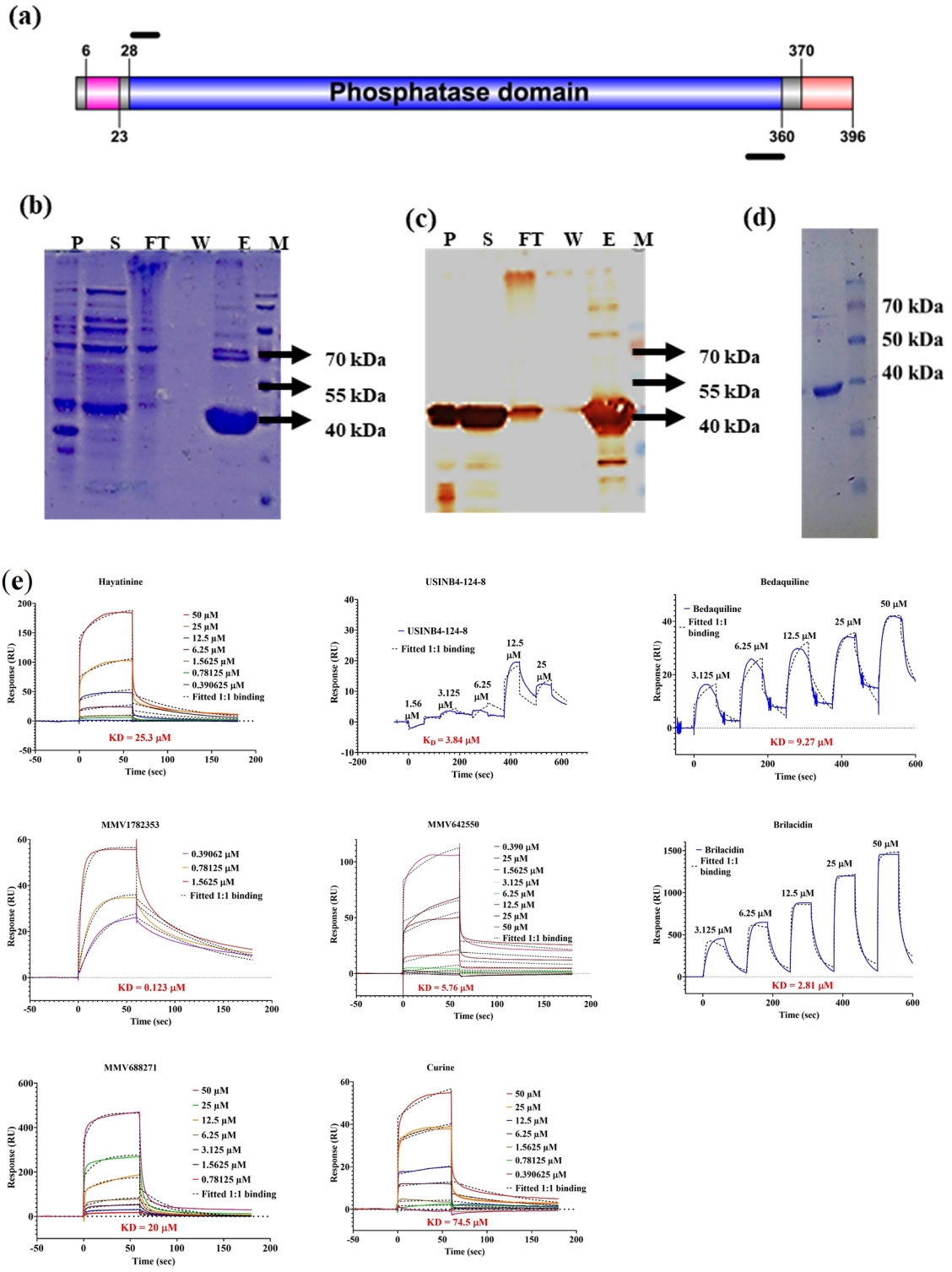

Figure 2. GAP50 expression and *in vitro* compound binding. (a) Graphical representation of domain organization of GAP50 showing an N-terminal signaling sequence followed by a phosphatase domain and C-terminal transmembrane domain; (b, c) coomassie and antihis antibody staining of purified GAP50 phosphatase domain *via* metal affinity chromatography; P: pellet, S: supernatant, FT: flow through, E: elution, and M: protein ladder. (d) GAP50 purity obtained after hydrophobic chromatography. (e) SPR sensorgrams representing compound interaction with GAP50 fitted with a 1:1 Langmuir binding model.

role as a scaffolding protein that anchors the glideosomal complex[30] to the inner membrane.[26,31] Although GAP50 is absent in humans and has been studied as a potential transmission-blocking vaccine candidate,[32] it has not yet been studied as an antimalarial drug target. The 1.7 Å resolution crystal structure of GAP50 by Bosch et al.[33] has further paved the way for antimalarial drug discovery by targeting this protein.

In the present study, we screened 951 different compounds from diverse chemical libraries against the *Pf*GAP50 protein using *in silico* computational, biophysical, and protein−drug

https://doi.org/10.1021/acsomega.3c05323
ACS Omega 2023, 8, 38506−38523

interaction tools. These compounds were shortlisted based on SPR analysis, their effect on *in vitro P. falciparum* culture, and their selectivity for malaria parasite. Further analysis of their role(s) at different asexual blood stages showed that these compounds act at different developmental stages. As *Pf*GAP50 is a component of the gliding machinery in different zoite forms of *Plasmodium*, it can be predicted that these compounds can act at multiple stages of the parasite. Bedaquiline, a highly active anti-MTB drug, was identified as an antiplasmodial in our screen and showed considerable antimalarial activity in the *in vivo Plasmodium berghei* mouse model. Thus, our findings provide new scaffolds/drug-like molecules that can act at different parasite developmental stages and can be a part of Artemsinin Combination Therapy (ACT).

RESULTS

Screening of MMV Box, Pandemic Box, and Other Synthetic Compounds Identified Eight Antimalarial Candidates That Target *Pf* Glideosome-Associated Protein GAP50. Since gliding machinery for different stages of *Plasmodium* spp. possesses some conserved proteins such as GAP45, GAP50, and several IMC proteins, we aimed to identify a common inhibitor that can block gliding at all of the lifecycle stages of *Plasmodium* spp. Here, we chose to target a conserved protein, *Pf*GAP50, that anchors surface proteins to IMC. Screening of 951 compounds (Figure 1a) from diverse chemical libraries like the pathogen box, pandemic box, Azepino quinolines, quinolines with β benzomorphan framework (Table S1), and secondary metabolites purified from *Cissampelos pareira*[34] for interactions with *Pf*GAP50 *via* Schrödinger drug discovery suite (version 2019−3), Differential Scanning Fluorimetry (DSF) followed by cell-based *in vitro* screening assays led to the identification of eight promising molecules (Figure 1b). In the absence of any known inhibitors and key binding sites on GAP50, permissive cutoff values for *in silico* screening were kept at −20 kcal/mol (MM-GBSA ΔG of binding), while a δT_m cutoff kept at ±2 °C was chosen for DSF-based screening to ensure that nothing was missed. The independent use of both *in silico* docking and DSF (δT_m) allowed us to select 345 of the 951 compounds.

Since both *in silico* docking and DSF can occasionally give false positives,[35−37] we used surface plasmon resonance[38] to validate the binding of the shortlisted 345 molecules to the recombinant *Pf*GAP50 protein immobilized on the CM5 chip. GAP50 consists of an N-terminal signaling sequence, followed by a phosphatase domain and a C-terminal transmembrane domain (Figure 1a). The phosphatase domain of GAP50 was expressed and purified to homogeneity in the soluble form using two chromatography steps: Ni-NTA$^+$ purification was followed by hydrophobic chromatography (Figure 2b−d).

Initial screening of 345 different molecules by SPR at 50 μM allowed the selection of 266 molecules that exhibited 1:1 binding with GAP50. Further, of these 266 molecules, 84 molecules were identified that were binding with GAP50 (K.D. < 100 μM) and were active against *Pf* (SI-2). Next, we screened all 84 molecules for their antiplasmodial IC_{50s} against different strains of the malarial parasite (Chloroquine-sensitive *Pf*3D7, Chloroquine-resistant *Pf*INDO, and Artemisinin-resistant *Pf*Cam3.1^{R539T} strains) (SI-2), leading to 39 compounds that showed IC_{50} against *P. falciparum* parasites of <20 μM for further toxicity testing against human kidney and liver cell lines, using the standard MTT assay.[39] Based on the selectivity index (>100-fold) for *P. falciparum* parasites, eight compounds (Hayatinine, Curine, MMV689758 (Bedaquiline), MMV1634402 (Brilacidin), and MMV688271, MMV782353, MMV642550, and USINB4-124-8) were selected for further analysis (Figure 1b). These molecules exhibited *Pf*GAP50 binding affinity of < 75 μM (Figure 2e) with IC_{50} against Chloroquine-sensitive and resistant strains <3 μM (Table 1). Notably, among the shortlisted molecules (Table 1), Bedaquiline, Brilacidin, MMV688271, MMV642550, and Hayatinine showed $IC_{50s} \leq 1.5$ μM against all three strains of *Plasmodium*. USINB4-124-8 and Hayatinine were found to be more active against *Pf*Cam3.1^{R539T} (IC_{50} 11.35 and 64.83 nM, respectively) than against the *Pf*INDO strain (IC_{50} 2.46 and 0.47 μM, respectively). In comparison, MMV1782353 and Curine showed $IC_{50} < 1$ μM for *Pf*INDO and *Pf*3D7 (Table 1) strains and exhibited IC_{50} values of >1 μM against *the Pf*Cam3.1^{R539T} strain. The differential activity observed for Hayatinine, Curine, MMV1782353, and USINB4-124-8 could be due to differential expression and modifications of protein(s) in different parasite strains, resulting in the alteration of parasite metabolic pathways.

Ring-Stage Survival Assay of Lead Molecules. Ring-stage Survival Assay[40] (RSA) was developed to analyze the effect of Artemisinin on the survival of early rings (0−3 h p.i.) in distinct parasite strains. To test the efficacy of the selected compounds at *the P. falciparum* ring stages, early rings (0−3 h p.i.) of ART-resistant strain (*Pf*Cam3.1^{R539T}) was treated with test molecules at their 10× IC_{50}, with Dihydroartemisinin and Artemisinin at 700 nM serving as positive controls. Among the eight compounds, Bedaquiline was the only molecule that showed activity against early rings (Figure 3). Hayatinine and USINB4-124-8 were found to have no effect on early rings despite having nanomolar activity against *Pf*Cam3.1^{R539T}. The results of the ring survival assay indicated that in addition to binding to *Pf*GAP50, these compounds may also target other parasite proteins, important for parasite survival. It is also possible that *Pf*GAP50 plays another role in addition to parasite gliding mobility.

IC_{50} Estimation of Selected Drugs against Asexual Blood Stages of *P. falciparum*. To explore the differential effect of lead antiplasmodial molecules on other asexual blood stages of *P. falciparum*, we subjected synchronized different cell cycle stages to each lead molecule at different concentrations for 12 h followed by evaluation of increased DNA content by SYBR green lysis as indicated in the method. As shown in Figure 4, there were marked differences in the observed IC_{50s} against different stages of these compounds. Taking early rings (E.R.) to late rings (L.R.), early trophozoites (E.T.) to late trophozoites (L.T.), early schizonts (E.S.) to late schizonts (L.S.), and late schizonts (L.S.) to early rings (E.R.) stages into consideration, USINB4-124-8 showed a much higher IC_{50} (μM) (38.12) against trophozoites and schizonts stages (54.32) than against rings (7.2). In contrast, MMV1782353 and MMV642550 showed significant activity ($IC_{50} < 5$ μM) against early and late schizonts, but less potency ($IC_{50} > 8$ μM) against rings (Figure 4). It is noteworthy that despite the remarkable structural resemblance, Hayatinine and Curine showed marked differences in activity against different asexual blood stages (Figure 1b). Thus, Hayatinine (608.7 Da) showed a marked preference for preventing the L.S. to E.R. transition. In contrast, Curine (594 Da) inhibited E.S. to L.S. transitions along with E.T. to L.T. transitions. In summary, except for USINB4-124-8, all other shortlisted molecules showed potent activity against the late trophozoite and schizont stages of *Pf*INDO parasites.

https://doi.org/10.1021/acsomega.3c05323
ACS Omega 2023, 8, 38506−38523

Table 1. *In Vitro* AntiPlasmodial IC_{50}, Mammalian Cell CC_{50}, Resistance Index (RI), and Selectivity Index (SI) of Top Eight *Pf*GAP50 Binders

Si. No.	Test molecule	IC_{50} (nM) against *Pf* strains			Resistance index[a]		CC_{50} (μM)		Selectivity index[b]	
		3D7	INDO	Cam3.1^{R539T}	*A*	*B*	HEK293	HUH-7	*A*	*B*
1.	Hayatinine	571.06 ± 63.8	470.03 ± 77.86	64.83 ± 8.90	0.82	0.16	37.3 ± 9.42	42.71 ± 4.22	90.84	104.00
2.	USINB4-124-8	225.5 ± 1.7	2469.5 ± 146.5	11.35 ± 1.09	8.96	0.02	>400	>400	>165.28	>165.28
3.	Bedaquiline	1205.66 ± 22.45	1009.2 ± 60.71	768.56 ± 73.61	0.89	0.59	>400	>400	366.97	366.97
4.	MMV1782353	669.65 ± 70.25	562.35 ± 171.35	14310 ± 210	0.64	21.25	>200	>200	500.00	500.00
5.	MMV642550	393.35 ± 6.45	985.6 ± 159.4	1401 ± 97	3.076	3.82	>200	>200	166.67	166.67
6.	Brilacidin	405.1 ± 63	634.35 ± 153.35	727.5 ± 65.2	1.48	1.92	>200	>200	298.51	298.51
7.	MMV688271	257.76 ± 54.2	283.96 ± 24.74	387.36 ± 39.64	0.75	1.02	119.1 ± 33.72	29.65 ± 3.76	478.31	119.08
8.	Curine	1509.33 ± 41.79	465.73 ± 50.83	3013.33 ± 269.14	0.34	1.91	104.1 ± 6.90	62.77 ± 6.60	204.1	123.07
9.	Chloroquine[c]	14 ± 5	290.0 ± 20	55.0 ± 4	20.71	3.92	45.69 ± 3.12	58.54 ± 4.73	157.55	201.86
10.	Artemisinin[c]	13.0 ± 4	10 ± 2	15 ± 2	0.77	1.15	>100	>100	>6666.66	>6666.66

[a]Resistance index (RI): A = IC_{50} *Pf*INDO/IC_{50} *Pf*3D7; B = IC_{50} *Pf*Cam3.1^{R539T}/IC_{50} *Pf*3D7. [b]Selectivity index (SI): A = CC_{50} HEK293/IC_{50} *Pf*INDO; B = CC_{50} *Pf*HUH7/IC_{50} *Pf*INDO. [c]Reference compounds. IC_{50} and CC_{50} values are presented as mean ± SEM (n = 3).

Deformities Induced by Lead Molecules on the Parasite Morphology. Post estimation of IC_{50} of selected molecules against different asexual cell stages of *P. falciparum*, their effects on parasite morphology, and development were studied further. Ring-stage parasites (6−12 h, p.i.) were treated for 57 h, and microscopic examination of Giemsa stained parasites was performed at 12, 36, 48, and 57 h (Figure 5a). Bedaquiline and Hayatinine permitted parasites to develop normally while preventing merozoites from invading. Thus, even after 57 h, the cultures treated with these two compounds displayed RBC surface-attached merozoites. In the case of Curine and Brilacidin treatments, merozoites adhering to RBC showed evidence of a partial suppression of invasion. MMV688271 inhibited schizont egression, whereas MMV1782353 and MMV642550 permitted *Pf* development at their respective IC_{50} values.

Together, these results indicate that despite being screened against the *Pf*GAP50 protein, which is specifically expressed during the late trophozoite stage, eight lead compounds differentially inhibited the development of different asexual blood stages of *P. falciparum*.

Differential Action of Lead Compounds on *P. falciparum* Merozoites Egression and Invasion. Since the rupture of schizonts and subsequent invasion of merozoites is a crucial step preceding the exponential increase in % parasitemia, molecules with IC_{50} < 10 μM against schizonts (Figure 4) were studied to examine (a) inhibition of egress of merozoites from schizonts and (b) merozoite invasion into healthy RBCs. Microscopic images of Giemsa-stained lead molecule treated parasites revealed that the presence of MMV molecules 1782353 and 642550 slowed the schizont rupture. After removal of MMV1782353 and 642550, schizonts ruptured and released merozoites, but none of the released merozoites could invade, leading to a decrease in % parasitemia (Figure 5b). Hayatinine treatment of schizonts for 8 h inhibited egress, with microscopic images showing many intact pyknotic schizonts and only a few RBC surface-attached merozoites. These merozoites were found noninvasive, as % parasitemia after removal of drugs was similar to that of heparin, a known inhibitor of invasion.[41] Curine allowed schizont egress, but the level of invasion was significantly reduced, suggesting that the treatment rendered the merozoites noninvasive. With no egress or invasion, both Bedaquiline and MMV688271 showed schizontocidal activity on mature (about to rupture) schizonts (Figure 5b).

These findings were confirmed by costaining the lead molecule-treated parasites with anti-PhiL antibody (IMC marker protein) and DAP1. Bedaquiline and Hayatinine, as shown in Figure 6a, inhibited gliding motility, thereby preventing cell invasion. Several unruptured schizonts were detected after Curine or MMV688271 treatment (Figure 6a). Schizogony was hampered in the case of Brilacidin, Curine, and MMV688271-treated parasites, as pyknotic schizonts were observed in the treated cultures. In summary, we found five compounds, Hayatinine, Bedaquiline, Brilacidin, Curine, and MMV688271, which completely prevented invasion/schizont rupture, whereas MMV1782353 and MMV642550 caused only partial inhibition of parasite invasion.

Blockade of Inner-Membrane Complex Formation by Lead Molecules. Since *Pf*GAP50 is a protein involved in forming IMC during schizogony and anchors several crucial surface proteins involved in invasion,[25] we next analyzed our lead GAP50 binders (IC_{50} against schizogony <10 μM) at their sublethal concentrations for their ability to perturb IMC

https://doi.org/10.1021/acsomega.3c05323
ACS Omega 2023, 8, 38506−38523

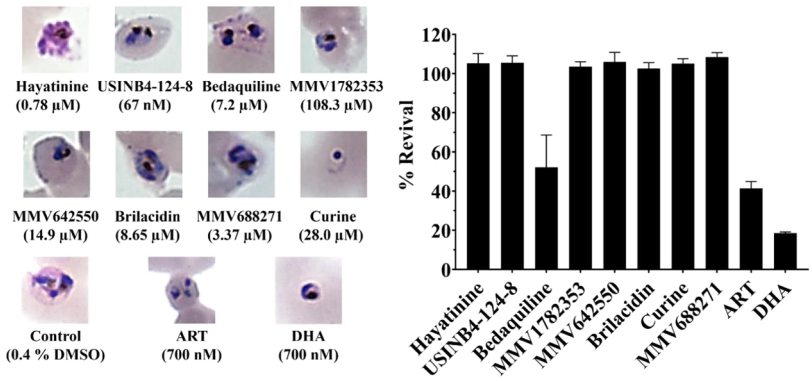

Figure 3. Evaluation of lead molecules (10× IC_{50}) in the ring-stage survival assay. Briefly, 0−3 h rings p.i. were treated for 6 h (10× IC_{50}), followed by test molecule removal by washing three times with 1× PBS and incubating in fresh cRPMI for the next 66 h. The left panel represents the microscopic evaluation of parasite morphology after 66 h of test molecule removal, whereas the right panel shows the percentage revival *via* the SYBR green lysis method. Bedaquiline kills 50% of early rings but does not affect stage progression. Hayatinine, Curine, and Brilacidin cause retardation in the growth cycle but are not able to kill early rings.

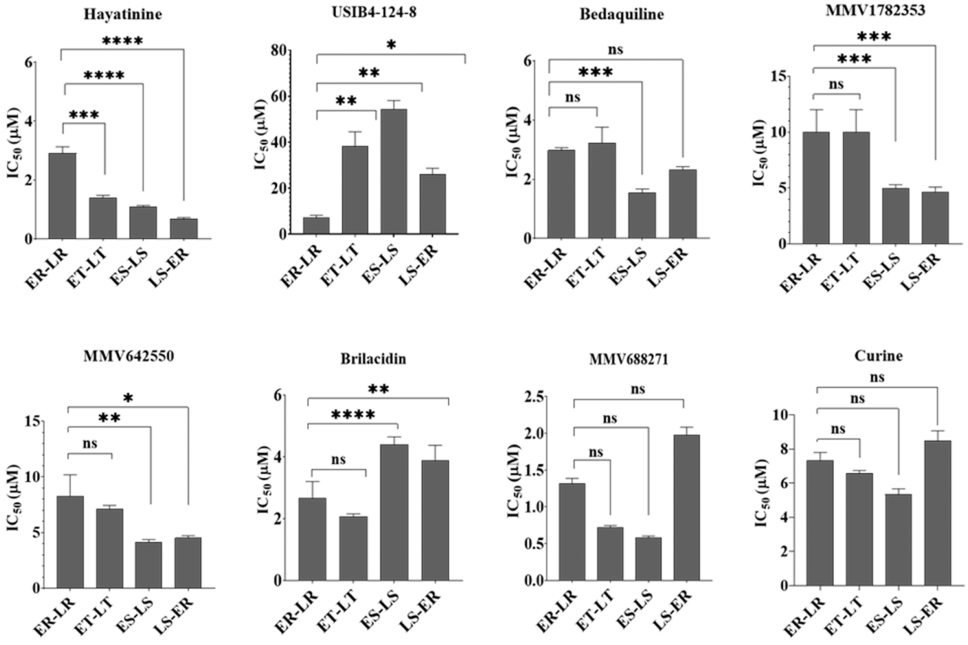

Figure 4. IC_{50} values of compounds against different asexual stages of *Pf* INDO. IC_{50} values of GAP50 binders against different stages of *Plasmodium*. E: early, L: late, R: rings, T: trophozoites, S: schizonts. All panels show the mean and standard deviation of triplicate experiments. In all three panels, a one-way ANNOVA was performed to estimate the *P* values: < 0.0212 (*), < 0.0082 (**), < 0.0008 (***), and < 0.0001 (****). "ns" denotes not significant.

formation. Recent publications[17,42] have shown colocalization of the GAP50 complex with the Phil1 complex at the schizont stage. These complexes have been shown to work in tandem to facilitate the process of invasion.[17,42] Hence, in control *vs* test molecule-treated schizonts, colocalization studies were performed for Phil1 and GAP50 proteins. As shown in Figure 6b, 0.4% DMSO-treated control *P. falciparum* schizonts displayed proper development of schizonts and near-complete colocalization of GAP50 and Phil1 ($P = 0.824$). Similar colocalization was observed in schizonts treated with MMV688271 (*P*-value = 0.886) and Curine ($P = 0.888$). In comparison, Hayatinine (*P*-value 0.617), Bedaquiline (*P*-value 0.641), and Brilacidin (*P*-value 0.613) disrupted IMC formation, affecting colocalization. Thus, the IMC disrupting activities of these compounds can be attributed to their ability to bind GAP50 or other proteins involved in proper IMC formation, thereby limiting its activity in gliding and invasion.

Based on compound IMC disruption and invasion-inhibitory activity, Bedaquiline, Hayatinine, Curine, MMV688271, and Brilacidin were selected for further studies.

Interaction of Lead Molecules with GAP50 as Seen through Molecular Dynamics (M.D.) Simulation. As seen in the docking studies, the eight lead molecules identified by us were found to bind at different sites on GAP50 (Figure 7). To understand the interaction stability of lead invasion-inhibitory compounds (Bedaquiline, Hayatinine, Curine, MMV688271, and Brilacidin) with the *Pf* GAP50 protein, M.D. stimulation studies were carried out post docking. According to the M.D. simulation, Bedaquiline was found to interact through hydrophobic interactions (contact residues: W35, I69, H256, and M278), hydrogen bonding (G65), and a water bridge (N221)

https://doi.org/10.1021/acsomega.3c05323
ACS Omega 2023, 8, 38506−38523

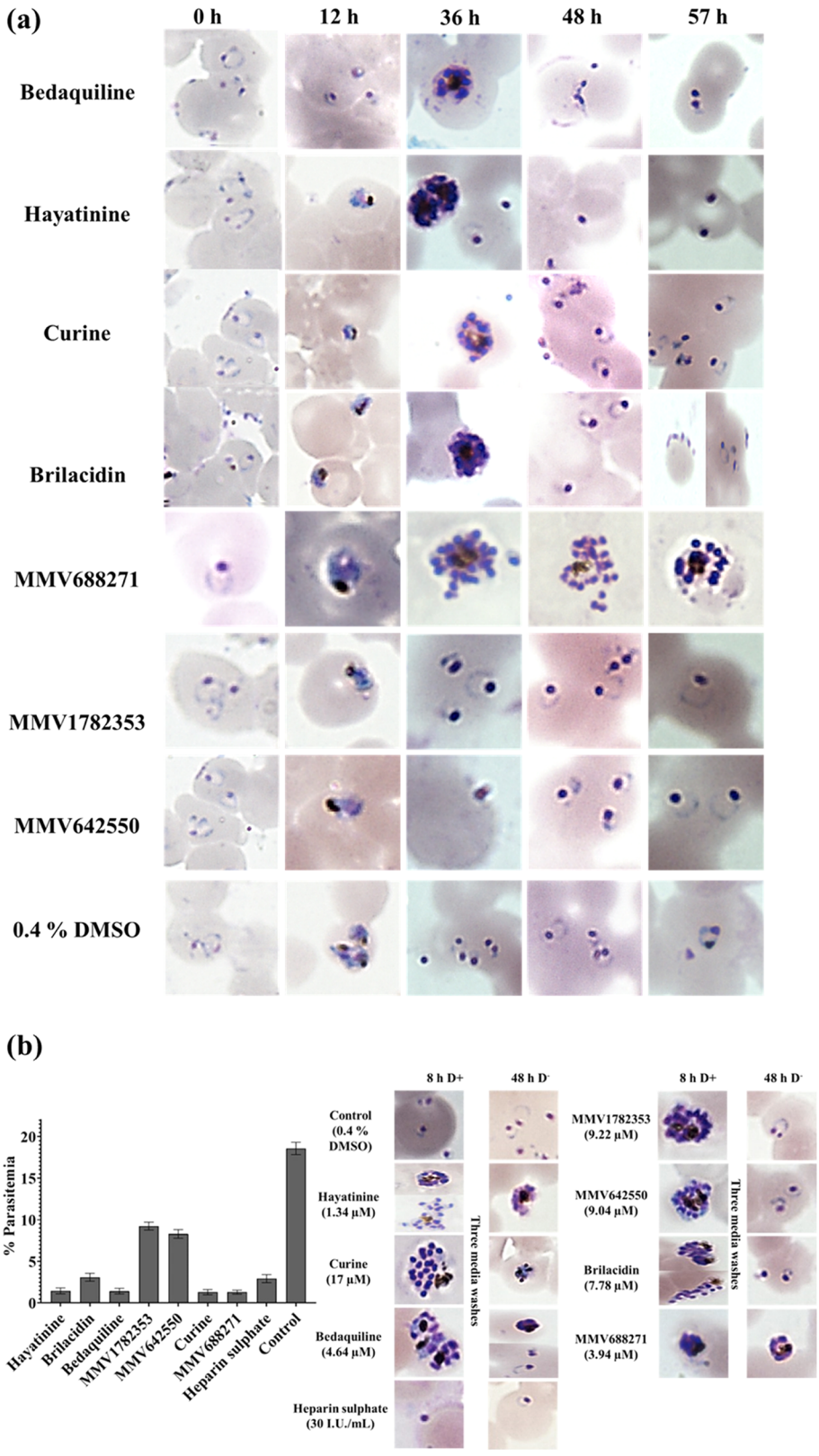

Figure 5. Effect of lead molecules on the asexual stages of *Pf*INDO. (a) Giemsa-stained images of *Pf*INDO cells treated with molecules at their IC_{50} for varying time intervals. Merozoites are seen attached but not invading RBCs in cultures treated with Bedaquiline, Hayatinine, and Brilacidin. MMV688271 treatment prevents schizont rupture. (b) Treatment of segmental-stage schizonts for 8 h with 2× IC_{50} (L.S. → E.R.), followed by replacement of test molecules using three centrifugal washes with cRPMI and growing parasites in cRPMI for the next 48 h. Left and right panels show microscopic evaluation and % parasitemia calculated by FACS (10^5 cells counted) analysis performed at the end of 56 h ($8D^+$ and $48D^-$), respectively. Heparin sulfate, a known invasion inhibitor, was used as a positive control. D^+ and D^- denote periods in the presence of test molecules, respectively.

https://doi.org/10.1021/acsomega.3c05323
ACS Omega 2023, 8, 38506−38523

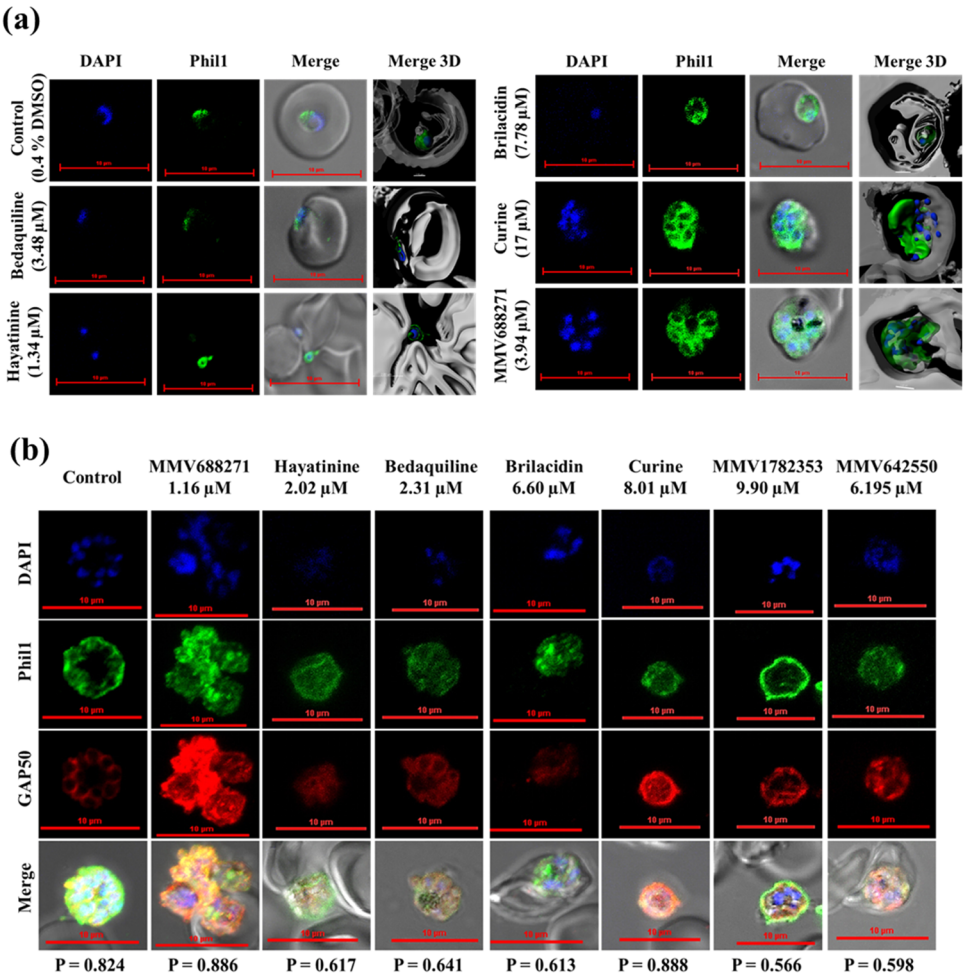

Figure 6. Effect of lead compounds on merozoite invasion and IMC formation. (a) Schizonts (34−36 h p.i.) were first treated with a sublethal concentration of test molecules for 12 h. The treated cultures were then subjected to DAPI staining (blue) and antibody-based staining of Phil1 (green) and GAP50 (red), as described in the Materials and Methods Section. The DAPI and antibody stained samples were examined by confocal imaging to find the effect of test molecules on the colocalization of these two proteins. 0.4% DMSO was used as a control. The *P*-values at the bottom are the Pearson correlation coefficients. (b) DAPI and immunofluorescence staining (Phil1) of 8 h test molecule-treated segmental schizonts. Notice the Phil1 staining inside the cell in control *vs* on the periphery in Bedaquiline and Hayatinine-treated cultures. Notice the remaining three schizontocidal molecules (Curine, Brilacidin, and MMV688271) exhibit massive schizont staining. Scale: 10 μM.

(Figures S1 and S2). These interactions were maintained over 30% of the 100 ns simulation time and appeared to be helping in stabilizing the binding of Bedaquiline with GAP50, resulting in −36.9 kcal/mol MM-GBSA ΔG of binding energy. Similar results obtained in SPR based binding study sensorgram profile obtained using a one-on-one interaction with *Pf*GAP50 indicated an SPR-based binding affinity (KD) of 9.27 μM (Figure 2e). The binding of Brilacidin with *Pf*GAP50 (Figures S3 and S4) was found to be primarily driven by water bridges mediated *via* the side chains and backbone of N127, E129, N148, D201, I322, N349, E351, and L352, which were further strengthened by hydrogen bond interactions involving E129, E351, and L352. Among these interactions, those with E129 and E351 were maintained for >50% of 100 ns simulation time (Figure S4). As many as 16 water bridges between Brilacidin and GAP50 may have contributed to the most promising MM-GBSA ΔG binding of −64.82 kcal/mol (SI-2), with a KD of 2.81 μM (SI-2).

Interactions of MMV688271 (Figures S5 and S6) with *Pf*GAP50 were stabilized through hydrogen bonds (E123, H152, F344, L347, P348), water bridges (E123, H152, F344, L347), and hydrophobic interactions (H152, F344, L347, V350). Varied interactions of MMV688271 with *Pf*GAP50 might explain why this compound showed a MM-GBSA ΔG binding of -41.86 kcal/mol with an *in vitro* KD of 20 μM. Interestingly, even though the structurally close Curine and Hayatinine bind to *Pf*GAP50, each binds to its unique site (Figures S7, S8, and S9). Furthermore, SPR revealed that the KD of Curine was nearly three times higher than that of Hayatinine, suggesting that the interaction of Hayatinine with *Pf*GAP50 is more robust than that with Curine (Figure 2e). Hayatinine was found to interact with G119, Q120, M146, P147, and H152 *via* water bridges and with E133 *via* hydrogen bonds (Figure S8). These bonds, which were found to persist for >30% of the simulation time, might prevent Hayatinine from moving out of its surface binding site (Figure S7b). Residues interacting with Curine (Figure S7c) *via* hydrogen bonds, hydrophobic interactions, and water bridges were Y96, L134, D135, D137, A138, V350, and E351. Our *in silico* docking and simulation studies predicted the binding interactions of lead molecules with GAP50, which can help in designing more potent and GAP50-specific inhibitors. However, structural data are required to confirm the binding modes and poses predicted by docking before the design of new inhibitors.

https://doi.org/10.1021/acsomega.3c05323
ACS Omega 2023, 8, 38506−38523

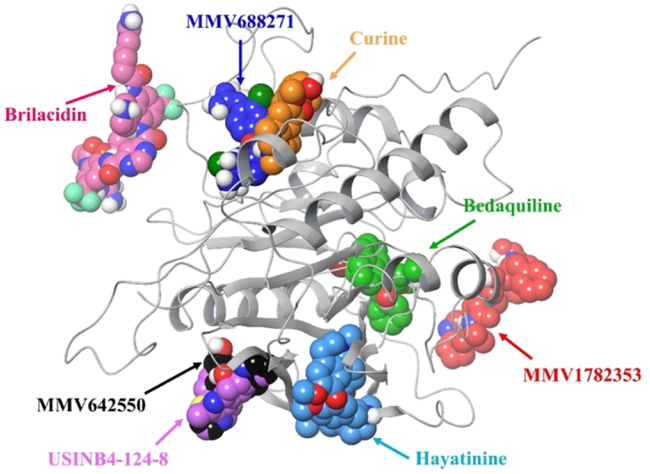

Figure 7. Representation of *in silico* binding sites of lead molecules against GAP50. The eight most promising molecules identified at the end of all filters used were found to bind to GAP50 at six different sites. Curine, Brilacidin, and MMV688271 (all binding at the top left edge of the molecule) were found to be schizontocidal, Hayatinine and Bedaquiline (binding at the bottom right) caused inhibition of invasion, while 1782353 and 642550 were schizontostatic since their withdrawal allowed the treated schizonts to egress and merozoites to invade. USINB4-12-8 showed a high IC_{50} against schizonts and was not pursued for its invasion-inhibitory activity.

The Activity of Lead Molecules in Combination with Other Antimalarials. To retard the development of resistance, reduce toxicity, and increase the efficacy of antimalarial drugs, it is preferable to use drug combination(s) to treat malaria. Hence, we evaluated the effect of five lead compounds that block invasion in combination with three current antimalarials (Pyrimethamine (PYR), Mefloquine (MFQ), and Artemisinin (ART)) on the *Pf*Cam3.1^{R539T} strain, which is ART, Sulfadoxine, and Pyrimethamine-resistant. As shown in Table S2, these drug combinations showed synergy ($\sum$FIC < 1), additivity (FIC > 1 < 2), and antagonism ($\sum$FIC < 2). When the $\sum$FIC values were averaged over varying ratios of drug combinations (Figure 8), the combinations of Hayatinine and Curine with Artemisinin turned out to be synergistic (average $\sum$FIC ≈ 0.5) and additive (average $\sum$FIC ≈ 1) with PYR and MFQ. Likewise, the average $\sum$FIC values for Bedaquiline, Brilacidin, and MMV688271 in combination with PYR, MFQ, and ART were additive. The additive/synergistic actions of these drugs in combination may be due to additional targets besides *Pf*GAP50 as a common target. This additive activity may allow the use of these compounds at their optimal concentrations with little risk of resistance development and fewer side effects/toxicities. Taken together, this study provides a basis for a new combination therapy that may be highly effective against drug-resistant strains of *P. falciparum*.

Putative Antiplasmodial Targets of Bedaquiline, Hayatinine, Brilacidin, MMV688271, and Curine. The submicromolar antiplasmodial IC_{50} of some of the compounds, together with μM KD against *Pf*GAP50, and multistage differential activity of invasion-inhibitory molecules led us to surmise that the malaria parasite proteome could have more targets in addition to *Pf*GAP50. Hence, invasion-inhibitory molecules from each library (Bedaquiline and MMV688271 (pathogen box), Brilacidin (pandemic box), Hayatinine, and Curine (phytometabolites from *C. pareira*)) were taken for cross-docking against 68 different malaria parasite proteins. The structures of these proteins were obtained from the PDB. Efforts were made to have the crystal structure of proteins inhibitor in bound form with resolution < 2.5 Å. The cocrystallized ligand of each of these proteins was docked to its respective protein to generate docking scores that were used as cut-offs for our lead molecules. Each lead molecule was docked into the active sites of the selected proteins, and docking scores was calculated. Of the 68 proteins studied (Table S3), the number of different protein−ligand complexes with docking scores < that of the cocrystallized ligand was 20 for MMV688271, 17 for Bedaquiline, 8 for Brilacidin, 7 for Hayatinine, and 10 for Curine (Tables S4−S8). Among the shortlisted proteins, three (Plasmepsins IV, Cyclophilin, and Malaria Sporozoite Protein Uis3) were common for all five molecules (Figure 9a,9b). These three targets are known to be expressed only in trophozoites and schizont stages[43] (Figure 9a), and binding of the test molecules to them might explain their cidal activity toward mature stages of *P. falciparum*. We also identified peptide deformylase, pyruvoyl tetrahydropterin synthase (PTPS), and glutaredoxin 1, which are uniquely expressed in trophozoites as putative targets of the test molecules (Figure 9a). To determine the binding affinity of our lead molecules for their putative target proteins, MM-GBSA ΔG binding was determined (Tables S4−S8). In all cases, ΔG binding was < −30 kcal/mol (Figure 9c). This low score suggests that the identified proteins may be targets of our lead molecules. However, extensive studies are required to confirm the status of these proteins as drug targets.

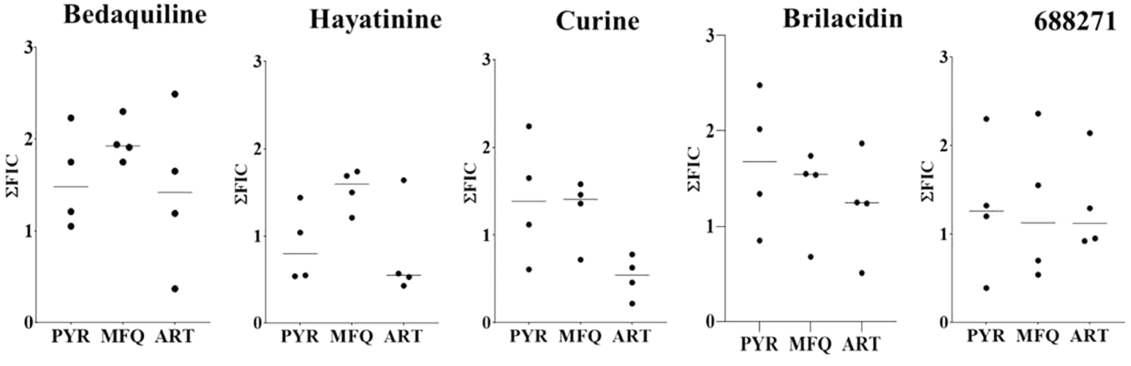

Figure 8. Graphical representation of $\sum$FIC values of lead molecules in combination with Pyrimethamine (PYR), Mefloquine (MFQ), and Artemisinin (ART). Each dot represents the $\sum$FIC of an individual ratio with horizontal bars indicating the mean values. Note the average $\sum$FIC values of ∼0.5 seen in combinations of Hayatinine and Curine with Artemisinin, indicating strong synergy.

https://doi.org/10.1021/acsomega.3c05323
ACS Omega 2023, 8, 38506−38523

(a)

Serial No.	PDB id	Protein	Stage expression	Compound
1	1LS5	Plasmepsin IV	Rings and merozites	Bedaquiline, Brilacidin, Curine, Hayatinine, MMV688271
2	1QNG	Cyclophilin	schizonts	Bedaquiline, Brilacidin, Curine, Hayatinine, MMV688271
3	2VWA	Malaria Sporozoite Protein Uis3	Schizonts	Bedaquiline, Brilacidin, Curine, Hayatinine, MMV688271
4	1RL4	Peptide Deformylase	trophozoites, gametocyte stage V	Bedaquiline, Brilacidin, Curine, MMV688272
5	1Y13	Pyruvoyl Tetrahydropterin Synthase(PTPS)	Trophozoites	Bedaquiline, Hayatinine, Curine, MMV688271
6	1Z6G	Guanylate Kinase	Late rings and Trophozites	Bedaquiline, Hayatinine, Curine, MMV688271
7	3PEH	HSP90	Trophozoites	Bedaquiline, Hayatinine, Curine, MMV688271
8	3AZB	Beta-Hydroxyacyl-Acyl Carrier Protein Dehydratase	Rings	Bedaquiline, Hayatinine, MMV688271
9	3QVI	Histo-Aspartic Protease (Hap)	Rings	Bedaquiline, Brilacidin, Curine
10	4MZB	PfGrx1	Trophozoties	Bedaquiline, Curine, MMV688271
11	2PMO	Ser/Thr protein kinase	Trophozoites and Schizonts	Bedaquiline, MMV688271
12	2YOG	Thymidylate Kinase	Schizonts, Gametocytes II, V	Bedaquiline, Curine
13	3C02	Aquaglyceroporin	Schizonts	Bedaquiline, Brilacidin
14	3K7Y	Aspartate Aminotransferase	Rings, Trophozoites	Bedaquiline, MMV688271

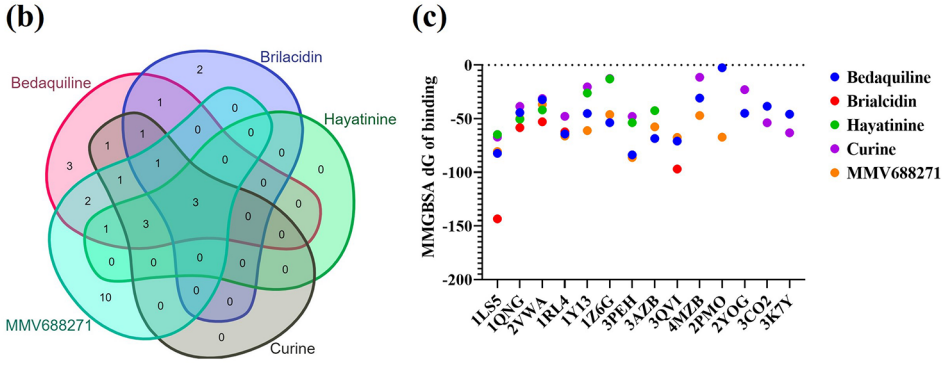

Figure 9. Cross-docking analysis of five invasion-inhibitory molecules. (a) Table showing malaria parasite proteins that showed *in silico* affinity for the five lead molecules; the stage of expression for target proteins was taken from Singh.[44] (b) Venn diagram showing the number of common targets. Note that the three proteins are common to Bedaquiline, Brilacidin, MMV688271, Curine, and Hayatinine. Unique proteins observed were 3 in Bedaquiline, 10 in MMV688271, 2 in Brilacidin, and none in the cases of Hayatinine and Curine. (c) MM-GBSA ΔG binding was observed for individual ligands with different proteins of the malaria parasite.

Bedaquiline Treatment Protects Mice in the *P. berghei* Mouse Model. Based on promising *in vitro* antiplasmodial potencies and selectivity indices (S.I.), we next tested the protective potential of Bedaquiline (50 mg/kg) and USINB4-124-8 (100 mg/kg) in an *in vivo P. berghei* mouse model. Briefly, seven mice in four groups were intraperitoneally injected with 10^5 *P. berghei* parasites. Parasitemia was monitored daily, and when it reached 1%, drug treatment was initiated. Each drug was administered orally for 4 consecutive days. The vehicle solution (2% (hydroxypropyl) methylcellulose with 2% Tween 80 in normal saline) was administered without the drug in the negative control group. Parasitemia was monitored daily for 40 days for each mouse. Treatment of *P. berghei ANKA* infected mice with vehicle solution (−ve control) led to increased fluctuations in body temperature and a decrease in mean body weight concomitant with the progressive increase in % Parasitemia with a median survival of 19 days and death of all 7 mice by day 22 (Figure 10). Likewise, USINB4-124-8 fed mice

https://doi.org/10.1021/acsomega.3c05323
ACS Omega 2023, 8, 38506−38523

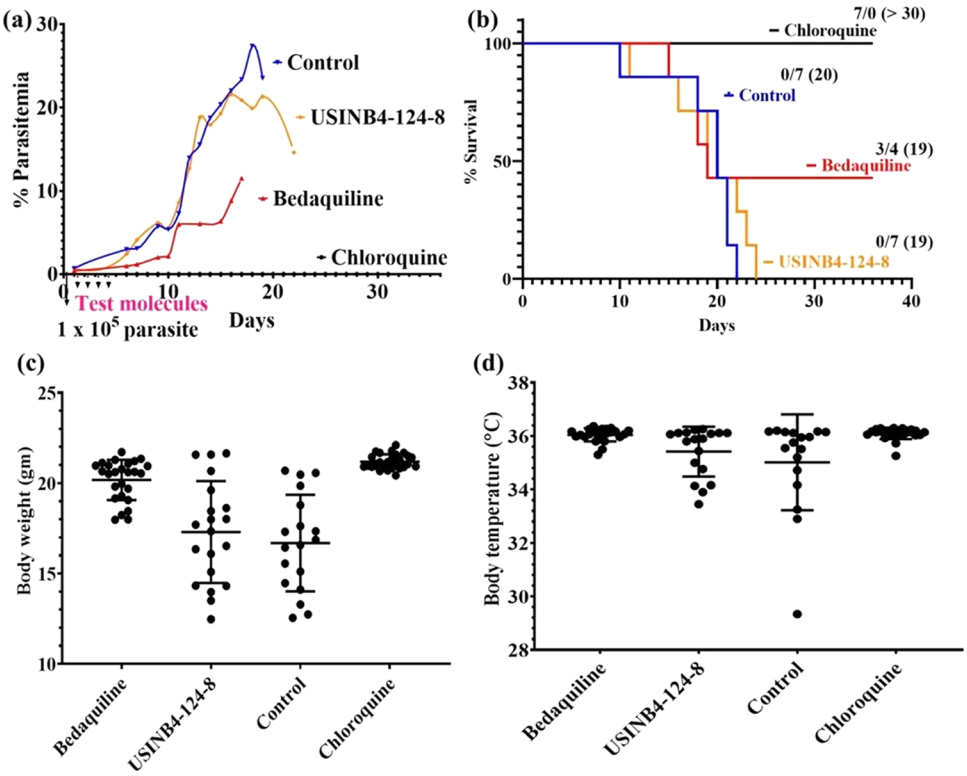

Figure 10. *In vivo* antimalarial effect of Bedaquiline and USINB4-124-8: (a) Mean % parasitemia; (b) median survival time. Superscripts in black indicate alive/dead mice with mean survival in parentheses; (c) changes in mean body weight and (d) change in mean temperature. Each dot in a group (C, D) represents a single day.

also showed no difference compared to the control in terms of survival, % increase in parasitemia, fluctuation in body weight, and temperature (Figure 10). Bedaquiline (50 mg/kg bwt) treatment resulted in complete suppression of % parasitemia by day 19, reduced temperature and body weight fluctuations compared to the control, with survival of three out of seven mice until 34 days (Figure 10). Together, these results showed partial protection of mice treated with a 50 mg/kg dose of Bedaquiline, thereby suggesting that Bedaquiline can be carefully considered for combination therapy, as well as for further chemical modifications. Bedaquiline is well tolerated at a 700 mg dosage in humans (C_{max} 6.47 mg/L) for MDR-TB treatment[45,46] and is known to clear TB infection in a mouse model at 25 mg/kg.[47] In the current study, Bedaquiline treatment at 50 mg/kg body weight for 4 days provided partial protection. It would be interesting to conduct future studies by increasing the dosage of Bedaquiline and tweaking its structure to determine whether this results in significant or complete protection in the *P. berghei* model of malaria.

DISCUSSION

The recent surge in malaria cases in Asia and Africa due to resistance to Chloroquine, sulfadoxine-pyrimethamine, ACT, and other antimalarial combinations necessitates the discovery of new antimalarials. Antigens on the surface and those involved in gliding *Plasmodium* zoites into host cells are important vaccine candidates and targets for new antimalarial discovery.[48−50] "Mosquirix" is the first sanctioned malaria vaccine based on one such antigen, called circumsporozoite protein (CSP) on the *Plasmodium* sporozoite surface. In this work, we used small compounds identified against *Pf*GAP50, a protein implicated in the gliding of different kinds of Plasmodium zoites, merozoites, sporozoites, and ookinetes into their respective host cells.[2,19,25,51] to target a *P. falciparum* blood stage asexual cycle. Despite differences in the cell morphology, *Plasmodium* motile forms at distinct lifecycle stages show similar gliding movements by linking their surface proteins with an intracellular actin−myosin motor. *Pf*GAP50 is a conserved protein at all *Plasmodium* motile stages that links surface proteins to the actin−myosin motor.[20,52]

Diverse drug-like compounds, along with some repurposed drugs from the medicines of malaria venture (MMV) pathogen and pandemic box,[53−55] were screened for their interactions with *Pf*GAP50 *via* the Schrödinger drug discovery suite (version 2019−3) and by differential scanning fluorimetry (DSF). High-affinity binders were further screened for their interaction with recombinant *Pf*GAP50 using SPR, their antiparasitic efficacy, and their toxicity against mammalian cells. Interestingly, our screening revealed many compounds as GAP50 binders that have previously been found to be promising against other pathogens. Notably, based on MMV's disease-based classification of compounds,[56−58] a few compounds (689437, 019189, 022029, 688371, 688271, 000016, and 000062) are already known for their antiprotozoal activity, while others such as Bedaquiline, 688775, 021660, and Brilacidin are known for their antibacterial activity. Similarly, 639951, 1782353, and 642550 are well-established antiviral agents (www.mmv.org/mmv-open). It should be noted that our work has, for the first time, identified Bedaquiline, Brilacidin, MMV642550, MMV688271, and MMV1782353 as promising agents against the malaria parasite. Among MMV FDA-approved molecules (KD GAP50 μM in parentheses), Mefloquine (40), Suramin (28.6), Bitertanol (0.333), Letermovir (19.2), Everolimus (0.257), Deferasirox (4.93), Valdecoxib (9.63), Ketoconazole (16.5),

https://doi.org/10.1021/acsomega.3c05323
ACS Omega 2023, 8, 38506−38523

Ezetimibe (1.16), LED 209 (2.62), Birinapant (12.4), Mgb Bp3 (14.8), Alexidine (27.0), Tipifarnib (52.2), Eberconazole (75.9), Ozanimod (76.5), Pentamidine (12.7), Rifampicin (0.116), Bedaquiline (9.27), and Brilacidin (2.81) have been identified as binders to *Pf*GAP50. All of these compounds belong to different chemical classes and are used for various purposes. Further, Mefloquine, Rifampicin, and Pentamidine identified as GAP50 binders were omitted from this study since their antimalarial activities and modes of action are well characterized.

Compounds with a binding affinity KD < 500 nM toward *Pf*GAP50 include Bitertanol, used as a fungicide,[59] Everolimus as a protein kinase inhibitor,[60] Ezetimibe as an inhibitor of HMG-CoA reductase,[61] and Rifampicin as an antibiotic with activity against both *Plasmodium*[62] and *Mycobacterium tuberculosis*.[63] After thorough screening, eight compounds, including Bedaquiline, Brilacidin (FDA-approved), MMV642550, MMV1782353 (pandemic box), MMV688271 (pathogen box), USINB4-124-8, Hayatinine, and Curine (*C. parreira*), were found to have high selectivity (>100) and low IC_{50} (<1 μM) against drug-resistant strains of *P. falciparum*. These molecules were selected for further evaluation of their effects at different *P. falciparum* asexual blood stages. Many of these identified compounds did not show a correlation between the SPR-based and *in silico* observed KD values. This can be attributed to several factors, including a lack of crystallographic knowledge about the compound binding site(s) on protein and the fact that *in silico* energy calculations take place in a vacuum environment where the protein and ligand(s) are treated as rigid molecules, whereas SPR interactions take place in a dynamic state with the protein and ligand surrounded by water molecules, leading to differential binding constants between these two techniques. Furthermore, SPR-based KD values of the identified compounds did not show a correlation with cell-based IC_{50} values. The likely cause of this discrepancy found an answer in our stage-specific assays that revealed the differential activity of these compounds against rings, trophozoites, and schizont stages of the parasite, although GAP50 expression is known to be the highest in schizonts. These selected compounds may interact with other Plasmodial proteins in addition to *Pf*GAP50, resulting in lower IC_{50} values than SPR-based KD values. Multistage activity is advantageous because it reduces the likelihood of resistance development if a compound targets multiple proteins/pathways.

Because the selection of these compounds was based on their ability to interact with *Pf*GAP50, a protein known to be involved in gliding as well as in IMC formation, these compounds were tested for their ability to block schizogony, egress, and invasion. Microscopic examination of Giemsa-stained parasites as well as by immunofluorescence analysis using anti-*Pf*GAP50 and anti-*Pf*PhiL antibodies revealed Bedaquiline, Hayatinine, Curine, MMV688271, and Brilacidin inhibited the schizogony, egress, and invasion of merozoites, as observed at different time points. In contrast, MMV compounds 1782353 and 642550 delayed schizont rupture. The observance of pyknotic or surface-attached merozoites which were unable to invade human RBCs, suggested merozoite development or gliding motility inhibition prevented merozoite entry into host cells. An indirect immunofluorescence assay was performed on lead molecule treated parasites with anti*Pf*GAP50 and anti-*Pf*PhiL1 antibodies to determine whether invasion was inhibited due to disruption of the precise architecture of IMC. Among these eight selected compounds, Brilacidin, Bedaquiline, Hayatinine, MMV1782353, and MMV642550 treatments disrupted IMC formation, which might be one of the reasons for their invasion inhibitory activity. Additionally, the effect of these molecules on schizont rupture could be attributed to their activity against phosphatases involved in egress because these compounds were selected based on their binding with the phosphatase domain of *Pf*GAP50. In short, we identified Bedaquiline, Hayatinine, Curine, MMV688271, and Brilacidin from eight shortlisted molecules that prevented schizont maturation, rupture, and invasion of merozoites. These selected compounds were docked to various proteins of the malarial parasite engaged in various cellular metabolic processes in a bid to investigate their mode of action on different stages of *Pf*. From 68 different proteins taken for docking, Plasmepsin IV, cyclophilin, glutaredoxins, and other vital targets were identified . It is well-known that the inhibition of these proteins causes cellular stress. Inhibiting Plasmepsin, for example, results in inhibiiton of hemoglobin digestion.[64] Similarly, inhibiting cyclophilin,[65] glutaredoxins,[66] and other important proteins identified as probable binders of our lead compounds may cause metabolic stress, disrupt cellular homeostasis, and lead to cell death.[67] Bedaquiline is known to promote electroneutral uncoupling of respiration-driven ATP synthesis[68] in *Mycobacterium tuberculosis* when the mode of action of lead compounds in diseases other than malaria is examined. Similarly, Brilacidin causes misfolding protein stress, as indicated by the upregulation of chaperones and proteases in Gram-negative and Gram-positive pathogens.[62] Since an increase in cellular stress levels has been shown to cause damage to cellular proteins, lipids, and nucleic acids, these selected compounds may cause parasite death by possibly similar mechanisms.[69] Although *Plasmodium* has evolved in diverse ways to maintain a state of homeostasis,[70] GAP50 binders may increase the stress inducer levels beyond the parasite's homeostatic ability, thus increasing the cellular stress, leading to the parasite's death.

These differential effects of the compounds seen in this work (Table S9) across different asexual stages of *Pf* may be due to interactions of these compounds with other *Plasmodium* proteins, due to different role(s) of *Pf*GAP50 or due to differences in GAP50 interactions with other proteins at different development stages. Indeed, many of these identified compounds can be starting points for developing future antimalarials. Interestingly, identifying these compound binding pockets using crystallographic methods in *Pf*GAP50 is expected to help us further in designing molecules with a strong affinity for *Pf*GAP50.

Coupled with over 100-fold selectivity, the presence of multiple targets in the malaria proteome is a plus point for these compounds since multitargeting drugs could have low chances of losing efficacy due to the development of resistance.

The finding of potent antiplasmodial activity in Bedaquiline and Brilacidin is highly significant since Bedaquiline is already being used against MDR-TB,[71] and Brilacidin is currently used in clinical trials as SARS-CoV2 drug. Further, identification of additive activity among standard antimalarials and FDA-approved antibacterials like Bedaquiline and Brilacidin, phytometabolites Hayatinine and Curine, and antifungal agent like MMV688271[72,73] might expedite their development as partner drugs with ART in Artemisinin combination therapy (ACTs).

In conclusion, this work has identified chemically diverse novel GAP50 binding molecules with promise against malaria and apicomplexan parasites . A notable feature of our work is

https://doi.org/10.1021/acsomega.3c05323
ACS Omega 2023, 8, 38506−38523

that it has for the first time led to the discovery of the putative binding pockets in GAP50. This can spur the application of computational tools to develop drugs that may bind to the sites identified in this work. Indeed, with the knowledge of binding sites, each of the new molecules we identified can be taken for future drug optimization and development as novel drugs against malaria. Although our studies have been mainly performed at asexual blood stages, it would be interesting to see these new series of compounds against other *Plasmodium* stages as *Pf*GAP50 is involved in gliding mobilities of all of the three *Plasmodium* zoite forms such as merozoite, ookinete, and sporozoite.

MATERIALS AND METHODS

Recombinant Expression and Affinity Purification of *Pf*GAP50. *Pf*3D7 genomic DNA was used to PCR amplify the *Pf*GAP50 gene using *Pf*GAP50 specific primers (5′-TTTTCATATGAAATGTCAACTACGCTTTGCG-3′-F.P.) and (5′-TTTGGATCCTTAATCTTTATTTCCCATGGGTCC-3′-R.P.). The amplified product was sequenced and cloned in the pET28a$^+$ vector, which was transformed into the Rosetta2 DE3 pLysS strain. 1% inoculum of the primary culture was used to initiate secondary culture supplemented with $CoSO_4$ (2 μM), kanamycin (50 μg/mL), and chloramphenicol (34 μg/mL).[33] Cells were induced with isopropyl β-D thiogalactopyranoside at 18 °C for 16 h. Harvested cells were lysed by sonication in buffer A (50 mM Tris HCl, pH 8.3, supplemented with 10% glycerol and 300 mM NaCl). Cellular debris was removed by centrifugation (13,000*g*, 45 min, 4 °C). The protein was purified by using metal affinity and hydrophobic interaction chromatography. The purified protein was dialyzed against the imidazole-free buffer and stored at 4 °C (up to 2 months).

***In silico* Docking, Molecular Dynamics Simulation, and $-\Delta G$ of Binding.** The PDB crystal structure of *Pf*GAP50 (ID: 3TGH) was prepared for docking using the protein preparation wizard[74] of Schrödinger software (version 19−3). Ligand structures drawn using ChemSketch (ver. 2021.1.2) software were imported into Schrödinger software. Ligprep[74] was used to prepare ligands for docking. Grid was generated to engulf the entire protein, and docking was carried out using the Glide module.[75] Docked poses were then taken to estimate $-\Delta G$ of binding using the Prime MM-GBSA module.[76] Lead *Pf*GAP50 binders (Bedaquiline, Hayatinine, Brilacidin, MMV688271, and Curine) that also showed good promise in *P. falciparum* culture-based study were taken for the molecular simulation study.[77] Briefly, the protein−ligand complex was solvated by using the TIP4PEW model in an orthorhombic box. Na^+ and Cl^- ions were added to neutralize the system. OPLS3e force field was used to simulate for 100 ns.

Compounds. Pathogen and Pandemic box compounds dissolved in DMSO at 10 mM were obtained from MMV. Azepino quinolines[78] and antiplasmodial molecules from *Cissampelos pareira*[34] were from Dr. Upendra Sharma, IHBT, India. The sources of these drug-like molecules were as follows: Bedaquiline (MMV689758) or HY-14881/CS-2921 (Med Chem Express), Mefloquine or M2319 and Bitertanol or 45349 (Sigma), Pentamidine or 20679 (Cayman chemicals), Suramin or 1874−250 (Bio vision), and MMV688771 or S14135SC (May bridge). Additionally, the MMV series of molecules 1634402 (Brilacidin), 1782353, 642550, and 688271 were procured from MMV.

Screening of Molecules Using Differential Scanning Fluorimetry. Recombinantly expressed and highly purified *Pf*GAP50 was used for *in vitro* small-molecule binding using differential scanning fluorimetry (DSF). Compounds were screened at 200 μM using 10 μM of the protein. DSF experiment was set up as described by Huynh and Partch.[79] T_m was calculated using a nonlinear regression model of Boltzmann Sigmoidal curve using the following equation

$$Y = \text{bottom} + (\text{top} - \text{bottom}) / \left\{1 + \exp\left(T_m - \frac{X}{\text{slope}}\right)\right\}$$

where Y is the fluorescence emission in arbitrary units; X is the temperature; Bottom is the baseline fluorescence at low temperature; Top is the maximal fluorescence; Slope is the the steepness of the curve; and T_m is the melting temperature of the protein. The binding of some small molecules may manifest as a decrease or an increase in protein stability. Molecules that gave a $\Delta T_m > 2.0$ °C over the solvent control were taken as potential hits.

Binding Affinity Determination Using Surface Plasmon Resonance. *Pf*GAP50 (50 μg/mL) was immobilized on a CM5 chip in acetate buffer, pH 4.5, using EDC-NHS coupling. Small test molecules were diluted in 1x PBS supplemented with 5% DMSO with 0.005% Polysorbate 20 (running buffer) to yield solutions of varying concentrations (2-fold serial dilution from 50 to 0.3125 μM) that were allowed to flow over the immobilized protein at a flow rate of 30 μL/min. Contact and dissociation times of 60 and 120 s, respectively, were given for each cycle. Regeneration was carried out using 10 mM glycine at pH 3.0. Data obtained was fitted with a 1:1 binding model to get K_a (association constant), K_d (dissociation constant), and K.D. (equilibrium binding affinity constant, aka equilibrium dissociation constant).

***In Vitro* Maintenance of *P. falciparum* Cultures and Assessment of Antiplasmodial Activity of Test Molecules.** Laboratory-adapted *Pf*3D7 (MRA102), *Pf*INDO (MRA819), and *Pf*Cam3.1^{R539T} (MRA1240) were procured from BEI resources and maintained in O^{+ve} human RBCs collected from the Rotary blood bank, New Delhi. Cultures at 4% hematocrit (H) were allowed to grow in complete RPMI 1640 medium at 37 °C under reduced O_2 (gas mixture: 5% O_2, 5% CO_2, and 90% N_2) as described by Trager and Jenson.[80] Antiplasmodial activities of test compounds were evaluated by fluorescence-based 96-well format SYBR green I assay as described. Growth inhibition studies were carried out in 96-well microtiter plates with final-well volumes of 100 μL (4 μL of test molecules and 96 μL parasite culture at 1% P and 2% H). After 72 hours, percent growth was determined by adding 100 μL of Lysis buffer (1x SYBR green, 20 mM Tris (pH 7.5), 5 mm EDTA, 0.008% (W/V) saponin, and 0.08% (v/v) Triton X-100). The plates were incubated in the dark for 2 hour at 37°C. Fluorescence was measured using wavelengths of 485 nm and 520 nm as excitation and emission, respectively. Chloroquine (4 μM) as zero growth positive control and 0.4% DMSO as 100% growth negative control was used. IC_{50} was calculated by plotting the inhibitor concentration *vs* normalized response and fitting the data with a nonlinear regression model in GraphPad Prism software.

***In Vitro* Cell Cytotoxicity Assay against Mammalian Cell Lines.** Human cell lines HUH-7 and HEK293 were used to determine the cytotoxic effects of test compounds by using MTT [3-(4,5-dimethylthiazol-2-yl)2,5-diphenyltetrazolium bromide] assay for mammalian cell viability as described by Mosmann.[39] Cells were cultured in 10% fetal bovine serum

https://doi.org/10.1021/acsomega.3c05323
ACS Omega 2023, 8, 38506−38523

supplemented with DMEM (cDMEM). Briefly, trypsinized cells (10^4 cells/200 μL cDMEM/well) were seeded in triplicate into 96-well flat-bottom tissue-culture plates. Following 16 h of cell seeding in triplicate, 200 μL of media was replaced with 96 μL of fresh cDMEM, and test molecule solutions (4 μL in 20% DMSO) were added. Culture plates were incubated for 24 h in a humidified atmosphere at 37 °C and 5% CO_2. 10 and 0.8% DMSO (v/v) were used as +ve (zero growth) and −ve (100% growth) controls, respectively. After 24 h treatment, 20 μL of MTT (5 mg/mL in 1× PBS) solution was added to each well, and plates were incubated for 4 h at 37 °C. After that, the plates were centrifuged (700*g*, 10 min), and supernatants were aspirated using a multipipet. This was followed by adding 200 μL of DMSO and incubating the plate at 37 °C for 10 min. The amount of formazan (a measure of cell growth) formed was assessed by measuring the optical density (OD) at 570 nm. CC_{50} was calculated by plotting the inhibitor concentration *vs* normalized response and fitting the data with a nonlinear regression model in GraphPad Prism software.

Ring-Stage Survival Assay (RSA). Ring-stage survival assay was carried out as per Witkowshi et al.[81] Briefly, *Pf*Cam3.1^{R539T} at 1% P rings (0−3 h p.i.) and 2% H were treated with 10× IC_{50} for 6 h followed by test molecule removal (three times using 1× PBS wash) and incubation in fresh cRPMI for the next 66 h. At the end of 72 h, stage progression was assessed by Giemsa-stained smear, and % revival was assessed by SYBR green I lysis method.

Stage-Specific Inhibition. *Pf*INDO cultures at 0−6 h post-invasion (p.i.) (rings), 18−22 h p.i. (trophozoites), 30−34 h p.i. (early schizonts), and 40−44 h p.i. (late schizonts) were incubated with varying concentrations of test molecules for a period of 12 h followed by test molecule removal by centrifugal media washes and allowing cultures to grow for second cycle (48 h) in test molecule free media. Plotting normalized growth curves and fitting them with nonlinear regression model yielded IC_{50} (concentration of test molecule at 50% growth) with untreated, and Chloroquine-treated cultures acting as 100% and 0% growth controls, respectively.

Egress/Invasion Inhibition Assay. This assay employed a late schizont to early ring (L.S. → E.R.) readout where late schizonts were treated with test molecules for 8 h followed by culture in test molecule free medium for a time sufficient to give rings in an untreated control culture. *Pf*INDO (42 to 45 h p.i.) culture was diluted to 1% P at 2% H in cRPMI and treated with test molecules at 2× IC_{50} for 8 h. This was followed by removing test molecules by three centrifugal washes with 1× PBS and incubating the washed cells in fresh cRPMI for 48 h. % P was calculated at the end of the second cycle using SYBR Green staining and counting 10^5 cells *via* FACS.

Evaluation of GAP50 Binder Antiplasmodial Molecules as Disruptors of Inner-Membrane Complex Formation and Invasion. We have used Phil1 and GAP50 antibodies to track the development of Schizont's inner-membrane complex (IMC) in the presence *vs* absence of the small test molecules that bind GAP50. Early schizonts (30−34 h p.i.) were treated with test compounds for 12 h, followed by indirect immunofluorescence assay (IFA) to assess IMC development. For this, cells were rinsed once with 1× PBS and fixed using a solution containing paraformaldehyde (4% v/v) and glutaraldehyde (0.0075% v/v) in PBS for 30 min. The fixed cells were treated with Triton X-100 (0.1% v/v) in 1× PBS (twice, 15 min each), and the permeabilized cells were blocked using BSA (4% w/v in 1× PBS). Parasites were then incubated with 1°Ab at 1:50 dilution overnight at 4 °C, followed by washing and incubation with 2°Ab (Alexa conjugated antirabbit antibody 488, Invitrogen) at 1:500 dilution for 3 h at R.T. In the end, DAPI (10 μg/mL) was used to stain the nucleus (10 min at R.T.). Samples were imaged using a Nikon A1-R confocal microscope. Similarly, segmented schizont cultures (42−45 h p.i.) were treated with test molecules for 8 h and evaluated *via* IFA for their ability to egress and the resulting merozoites to invade healthy red blood cells leading to the formation of rings.

***In Vitro* Potency of the Combinations of Lead Antiplasmodial Molecules.** To determine the effect of combining drugs on potency, different drug combinations were made to determine IC_{50} of combinations against the synchronous ring stage (6−12 h p.i., at 1% P and 2% H) of *P. falciparum* (MRA1240) in culture. 8× IC_{50} of each test molecule in 10% DMSO/1× PBS was taken as stock (A) and mixed with 8× IC_{50} of standard antimalarials (B) in four different molar ratios (4:1, 3:2, 2:3, and 1:4). Each ratio sample was further serially 2-fold diluted in 10% DMSO/1× PBS. Four microliters of each dilution was mixed with 96 μL of parasite culture (1% P, 2% H). Thus, each experimental well contained a total volume of 100 μL with or without test molecules. Control (0.4% DMSO (v/v)) that is nontoxic to the parasite was used as −ve control (100% growth), while Chloroquine (4 μM) was used as +ve control (0% growth). The plates were incubated (37 °C, 72 h), followed by an estimation of parasite proliferation using the SYBR Green I lysis method. Data analysis was done as described by Thapar et al.[82] The sum of Fractional inhibitory concentrations ($\sum$FIC) was calculated as $FIC_A + FIC_B$, where FICs are $FIC_A = IC_{50}$ of A in combination/IC_{50} of A when alone; $FIC_B = IC_{50}$ of B in combination/IC_{50} of B alone. The sum of FICs $\sum FIC = FIC_A + FIC_B$ was used to classify interactions[83] as strongly synergistic ($\sum FIC \leq 0.5$), weakly synergistic ($\sum$FIC 0.5−1), additive ($\sum$FIC 1−2.0), or antagonistic ($\sum FIC > 2.0$).

***In Vivo* Antimalarial Study.** *In vivo* antimalarial study was carried out per ARRIVE guidelines 2.0 with prior permission from ICGEB animal ethical committee (ICGEB/IAEC/30012021/MPB-8). Briefly, 10^5 *P. berghei ANKA* infected RBCs were injected into mice (6−8 weeks old, male, average weight 20 ± 2 g) and grouped randomly with seven mice/group. After infection establishment, test molecules were orally administered in vehicle solution (2% (hydroxypropyl) methylcellulose with 2% Tween 80 in normal saline) for 4 consecutive days, followed by daily monitoring of % P, body weight, and body temperature. Chloroquine (50 mg/kg b. wt.) was taken as the +ve control.

■ ASSOCIATED CONTENT

Data Availability Statement

The manuscript and its Supporting Information files contain all necessary data.

Supporting Information

The Supporting Information is available free of charge at https://pubs.acs.org/doi/10.1021/acsomega.3c05323.

Structures of in-house synthetic (quinolines and Azepino) molecules (Table S1); *in silico* binding of Bedaquiline to GAP50 seen at the end of 100 ns MD simulation, pictorial representation of (a) water bridges between ligand and protein, (b) binding cavity of ligand, (c) binding site residues, and (d) RMSD plot of the protein and ligand during the course of 100 ns simulation (Figure S1); interaction mapping of Bedaquiline with GAP50, (a)

https://doi.org/10.1021/acsomega.3c05323
ACS Omega 2023, 8, 38506−38523

interaction type between amino acids of GAP50 and Bedaquiline (Figure S2); *in silico* binding of Brilacidin to GAP50 seen at the end of 100 ns MD simulation, pictorial representation of (a) water bridges between the ligand and protein, (b) binding cavity of the ligand, (c) binding site residues, and (d) RMSD plot of the protein and ligand during the course of 100 ns simulation (Figure S3); interaction mapping of Brilacidin with GAP50, (a) interaction type between amino acids of GAP50 and Brilacidin (Figure S4); *in silico* binding of MMV688271 to GAP50 seen at the end of 200 ns MD simulation, pictorial representation of (a) water bridges between ligand and protein, (b) binding cavity of ligand, (c) binding site residues, and (d) RMSD plot of protein and ligand during the course of 200 ns simulation (Figure S5); interaction mapping of MMV688271 with GAP50, (a) interaction type between amino acids of GAP50 and MMV688271 (Figure S6); *in silico* determination of the interaction type and its stability between *C. pareira* lead molecules and GAP50, (a) level of different interactions (hydrogen bond, water bridges, *etc.*,) between Hayatinine and amino acid residues of GAP50, (b) RMSD deviation of Hayatinine bound with GAP50 (red curve), (c) level of different bond formation between Curine and GAP50, (d) RMSD deviation of Curine with respect to GAP50, note, with similar structure of both these compounds, they are interacting with different amino acids of GAP50 and are having a dissimilar protein−ligand RMSD plot (Figure S7); *in silico* interactions of Hayatinine with *Pf*GAP50 as seen at the end of 100 ns MD simulation, (a) involvement of water molecules in stabilizing the binding of Hayatinine, (b) binding cavity of Hayatinine (note: Hayatinine is bridging two different regions of the protein), (c) amino acid residue constituting the Hayatinine binding region (Figure S8); *in silico* interaction of curine with *Pf*GAP50 as seen at the end of 200 ns MD simulation, (a) involvement of water molecules in bridging association between Curine and GAP50, (b) binding cavity of Curine, and (c) amino acid residue constituting the binding region (Figure S9); FIC, ∑FIC, and Mean ∑FIC of lead compounds in combination with standard antimalarial drugs (Table S2); details of malaria proteins taken for cross-docking to identify alternate targets for GAP50 inhibitors (Table S3); proteins interacting with MMV688271, their docking score, and MM-GBSA dG of the binding score (Table S4); proteins interacting with Bedaquiline, their docking score, and MM-GBSA dG of the binding score (Table S5); proteins interacting with Brilacidin, their docking score, and MM-GBSA dG of the binding score (Table S6); proteins interacting with Hayatinine, their docking score, and MM-GBSA dG of the binding score (Table S7); proteins interacting with Curine, their docking score, and MM-GBSA dG of the binding score (Table S8); and differential activity of top eight compounds (Table S9) (PDF)

Quinoline derivatives: *in vitro* activity of quinoline derivative found to be interacting with GAP50; S2-phytometabolites: *in vitro* activity of *C. pareira* phytometabolites found to be interacting with GAP50; S2-Pandemic box: *in vitro* activity of MMV Pandemic box compounds found to be interacting with GAP50; S2-Pathogen box: *in vitro* activity of MMV Pathogen box compounds found to be interacting with GAP50 (XLSX)

AUTHOR INFORMATION

Corresponding Authors

Prakhar Agrawal − *International Centre for Genetic Engineering and Biotechnology, New Delhi 110067, India;* orcid.org/0000-0003-3641-4814; Email: agrawalprakhar03@gmail.com

Pawan Malhotra − *International Centre for Genetic Engineering and Biotechnology, New Delhi 110067, India;* orcid.org/0000-0002-7384-6280; Email: pawanmal@gmail.com

Authors

Surekha Kumari − *Chemical Technology Division, CSIR-Institute of Himalayan Bioresource Technology, Palampur 176061, India; Academy of Scientific and Innovative Research (AcSIR), Ghaziabad, Uttar Pradesh 201002, India*

Asif Mohmmed − *International Centre for Genetic Engineering and Biotechnology, New Delhi 110067, India*

Upendra Sharma − *Chemical Technology Division, CSIR-Institute of Himalayan Bioresource Technology, Palampur 176061, India; Academy of Scientific and Innovative Research (AcSIR), Ghaziabad, Uttar Pradesh 201002, India;* orcid.org/0000-0002-7693-8690

Dinkar Sahal − *International Centre for Genetic Engineering and Biotechnology, New Delhi 110067, India*

Complete contact information is available at: https://pubs.acs.org/10.1021/acsomega.3c05323

Author Contributions

P.A. and D.S. contributed to conceptualizing the idea and writing of the manuscript. P.A. did all experiments and data analysis. S.K. and U.S. provided pure synthetic quinoline derivatives and phytometabolites for this work. P.M., A.M., and U.S. contributed to the writing, proofreading, and organization of the manuscript.

Funding

P.A. and S.K. gratefully acknowledge financial support from the Department of Biotechnology, Government of India, and CSIR, New Delhi, respectively, in the form of JRF and SRF fellowships. This work was financially supported by ICGEB, New Delhi, in the form of the core grant to the Malaria Drug Discovery and Malaria Biology Groups. P.M. is the recipient of JC Bose Fellowship awarded by SERB, Govt. Of India and a part of this work is supported by grant DST/20/015.

Notes

The authors declare no competing financial interest.

ACKNOWLEDGMENTS

The authors are thankful to MMV for providing pathogen and pandemic box compounds and Dr. Purnima and Dr. Swati Gupta for helping with confocal experiments. The authors thank Dr. Arockiasamy Arulandu and Dr. Shobhan Kuila for helping with SPR and *in silico* Schrödinger's work.

ABBREVIATIONS

ART:Artemisinin; b.wt:body weight; DHA:Dihydroartemisinin; CC_{50}:concentration that causes 50% growth inhibition in human cell lines; E.S.:early schizont; E.T.:early trophozoite; GAP:glideosome-associated protein; IC_{50}:concentration that causes 50% growth inhibition of malaria parasite.; IMC:inner-

https://doi.org/10.1021/acsomega.3c05323
ACS Omega 2023, 8, 38506−38523

membrane complex; L.S.:late schizont; L.T.:late trophozoite; MFQ:mefloquine; MM-GBSA:molecular mechanics generalized born surface area; MMV:medicines for malaria venture; p.i.:postinvasion; PYR:pyrimethamine; R:rings; RBC:red blood cell; RI:resistance index; SPR:surface plasmon resonance; S:schizonts; SI:selectivity index; T:trophozoites

REFERENCES

(1) Baum, J.; Gilberger, T. W.; Frischknecht, F.; Meissner, M. Host-cell invasion by malaria parasites: insights from Plasmodium and Toxoplasma. *Trends Parasitol.* **2008**, *24*, 557−563.

(2) Kappe, S.; Bruderer, T.; Gantt, S.; et al. Conservation of a gliding motility and cell invasion machinery in Apicomplexan parasites. *J. Cell Biol.* **1999**, *147*, 937−943.

(3) Kappe, S. H. I.; Buscaglia, C. A.; Bergman, L. W.; Coppens, I.; Nussenzweig, V. Apicomplexan gliding motility and host cell invasion: Overhauling the motor model. *Trends Parasitol.* **2004**, *20*, 13−16.

(4) Heintzelman, M. B. Gliding motility in apicomplexan parasites. *Semin. Cell Dev. Biol.* **2015**, *46*, 135−142.

(5) Blank, A.; Fürle, K.; Jäschke, A.; et al. Immunization with full-length Plasmodium falciparum merozoite surface protein 1 is safe and elicits functional cytophilic antibodies in a randomized first-in-human trial. *npj Vaccines* **2020**, *5*, No. 10, DOI: 10.1038/s41541-020-0160-2.

(6) Genton, B.; Al-Yaman, F.; Betuela, I.; et al. Safety and immunogenicity of a three-component blood-stage malaria vaccine (MSP1, MSP2, RESA) against Plasmodium falciparum in Papua New Guinean children. *Vaccine* **2003**, *22*, 30−41.

(7) Thera, M. A.; Doumbo, O. K.; Coulibaly, D.; et al. A Field Trial to Assess a Blood-Stage Malaria Vaccine. *N. Engl. J. Med.* **2011**, *365*, 1004−1013.

(8) Payne, R. O.; Silk, S. E.; Elias, S. C.; et al. Human vaccination against RH5 induces neutralizing antimalarial antibodies that inhibit RH5 invasion complex interactions. *JCI Insight* **2017**, *2*, No. e96381, DOI: 10.1172/jci.insight.96381.

(9) Koram, K. A.; Adu, B.; Ocran, J.; et al. Safety and immunogenicity of EBA-175 RII-NG Malaria vaccine administered intramuscularly in semi-immune adults: A Phase 1, Double-blinded placebo controlled dosage escalation study. *PLoS One* **2016**, *11*, No. e0163066, DOI: 10.1371/journal.pone.0163066.

(10) Bhowmick, I. P.; Kumar, N.; Sharma, S.; Coppens, I.; Jarori, G. K. Plasmodium falciparum enolase: Stage-specific expression and sub-cellular localization. *Malar. J.* **2009**, *8*, No. 179, DOI: 10.1186/1475-2875-8-179.

(11) Duraisingh, M. T.; DeSimone, T.; Jennings, C.; Refour, P.; Wu, C. Erythrocyte invasion by Plasmodium falciparum: Multiple ligand-receptor interactions and phenotypic switching. *Subcell. Biochem.* **2008**, *47*, 46−57.

(12) Frénal, K.; Dubremetz, J. F.; Lebrun, M.; Soldati-Favre, D. Gliding motility powers invasion and egress in Apicomplexa. *Nat. Rev. Microbiol.* **2017**, *15*, 645−660, DOI: 10.1038/nrmicro.2017.86.

(13) Boucher, L. E.; Bosch, J. The apicomplexan glideosome and adhesins - Structures and function. *J. Struct. Biol.* **2015**, *190*, 93−114.

(14) Qian, P.; Wang, X.; Zhong, C. Q.; et al. Inner membrane complex proteomics reveals a palmitoylation regulation critical for intra-erythrocytic development of malaria parasite. *eLife* **2022**, *11*, No. e77447, DOI: 10.7554/eLife.77447.

(15) Harding, C. R.; Egarter, S.; Gow, M.; et al. Gliding Associated Proteins Play Essential Roles during the Formation of the Inner Membrane Complex of Toxoplasma gondii. *PLoS Pathog.* **2016**, *12*, No. e1005403, DOI: 10.1371/journal.ppat.1005403.

(16) Poulin, B.; Patzewitz, E. M.; Brady, D.; et al. Unique apicomplexan IMC sub-compartment proteins are early markers for apical polarity in the malaria parasite. *Biol. Open* **2013**, *2*, 1160−1170.

(17) Saini, E.; Sheokand, P. K.; Sharma, V.; et al. Plasmodium falciparum PhIL1-associated complex plays an essential role in merozoite reorientation and invasion of host erythrocytes. *PLoS Pathog.* **2021**, *17*, No. e1009750, DOI: 10.1371/journal.ppat.1009750.

(18) Gao, H.; Yang, Z.; Wang, X.; et al. ISP1-Anchored Polarization of GCβ/CDC50A Complex Initiates Malaria Ookinete Gliding Motility. *Curr. Biol.* **2018**, *28*, 2763−2776.e6, DOI: 10.1016/j.cub.2018.06.069.

(19) Frénal, K.; Soldati-Favre, D. [The glideosome, a unique machinery that assists the Apicomplexa in gliding into host cells]. *Med. Sci.: M/S* **2013**, *29*, 515−522.

(20) Yeoman, J. A.; Hanssen, E.; Maier, A. G.; et al. Tracking glideosome-associated protein 50 reveals the development and organization of the inner membrane complex of Plasmodium falciparum. *Eukaryotic Cell* **2011**, *10*, 556−564.

(21) Boucher, L. E.; Bosch, J.Glideosome of Apicomplexans as a Drug Target. In *Comprehensive Analysis of Parasite Biology: From Metabolism to Drug Discovery*; Wiley, 2016; pp 255−274.

(22) Parkyn Schneider, M.; Liu, B.; Glock, P.; et al. Disrupting assembly of the inner membrane complex blocks Plasmodium falciparum sexual stage development. *PLoS Pathog.* **2017**, *13*, No. e1006659.

(23) Ferreira, J. L.; Heincke, D.; Wichers, J. S.; et al. The Dynamic Roles of the Inner Membrane Complex in the Multiple Stages of the Malaria Parasite. *Front. Cell. Infect. Microbiol.* **2021**, *10*, No. 611801, DOI: 10.3389/fcimb.2020.611801.

(24) Opitz, C.; Soldati, D. 'The glideosome': A dynamic complex powering gliding motion and host cell invasion by Toxoplasma gondii. *Mol. Microbiol.* **2002**, *45*, 597−604.

(25) Baum, J.; Richard, D.; Healer, J.; et al. A conserved molecular motor drives cell invasion and gliding motility across malaria life cycle stages and other apicomplexan parasites. *J. Biol. Chem.* **2006**, *281*, 5197−5208.

(26) Gaskins, E.; Gilk, S.; DeVore, N.; et al. Identification of the membrane receptor of a class XIV myosin in Toxoplasma gondii. *J. Cell Biol.* **2004**, *165*, 383−393.

(27) Dearnley, M. K.; Yeoman, J. A.; Hanssen, E.; et al. Origin, composition, organization and function of the inner membrane complex of Plasmodium falciparum gametocytes. *J. Cell Sci.* **2012**, *125*, 2053−2063.

(28) Cowman, A. F.; Berry, D.; Baum, J. The cellular and molecular basis for malaria parasite invasion of the human red blood cell. *J. Cell Biol.* **2012**, *198*, 961−971.

(29) Bergman, L. W.; Kaiser, K.; Fujioka, H.; et al. Myosin A tail domain interacting protein (MTIP) localizes to the inner membrane complex of Plasmodium sporozoites. *J. Cell Sci.* **2003**, *116*, 39−49.

(30) Soldati-Favre, D. Molecular dissection of host cell invasion by the Apicomplexans: The glideosome. *Parasite* **2008**, *15*, 197−205.

(31) Cowman, A. F.; Baldi, D. L.; Healer, J.; et al. Functional analysis of proteins involved in Plasmodium falciparum merozoite invasion of red blood cells. *FEBS Lett.* **2000**, *476*, 84−88.

(32) Beiss, V.; Spiegel, H.; Boes, A.; et al. Plant expression and characterization of the transmission-blocking vaccine candidate PfGAP50. *BMC Biotechnol.* **2015**, *15*, No. 108, DOI: 10.1186/s12896-015-0225-x.

(33) Bosch, J.; Paige, M. H.; Vaidya, A. B.; Bergman, L. W.; Hol, W. G. J. Crystal structure of GAP50, the anchor of the invasion machinery in the inner membrane complex of Plasmodium falciparum. *J. Struct. Biol.* **2012**, *178*, 61−73.

(34) Bhatt, V.; Kumari, S.; Upadhyay, P.; et al. Chemical profiling and quantification of potential active constituents responsible for the antiplasmodial activity of Cissampelos pareira. *J. Ethnopharmacol.* **2020**, *262*, No. 113185.

(35) Gao, K.; Oerlemans, R.; Groves, M. R. Theory and applications of differential scanning fluorimetry in early-stage drug discovery. *Biophys. Rev.* **2020**, *12*, 85−104.

(36) Sink, R.; Gobec, S.; Pecar, S.; Zega, A. False Positives in the Early Stages of Drug Discovery. *Curr. Med. Chem.* **2010**, *17*, 4231−4255.

(37) Davis, B. J.; Erlanson, D. A. Learning from our mistakes: The 'unknown knowns' in fragment screening. *Bioorg. Med. Chem. Lett.* **2013**, *23*, 2844−2852.

(38) Bakhtiar, R. Surface plasmon resonance spectroscopy: A versatile technique in a biochemist's toolbox. *J. Chem. Educ.* **2013**, *90*, 203−209.

https://doi.org/10.1021/acsomega.3c05323
ACS Omega 2023, 8, 38506−38523

(39) Mosmann, T. Rapid colorimetric assay for cellular growth and survival: Application to proliferation and cytotoxicity assays. *J. Immunol. Methods* **1983**, *65*, 55−63.
(40) Zhang, J.; Feng, G.-H.; Zou, C. Y.; et al. Overview of the improvement of the ring-stage survival assay-a novel phenotypic assay for the detection of artemisinin-resistant Plasmodium falciparum. *Zool. Res.* **2017**, *38*, 317−320, DOI: 10.24272/j.issn.2095-8137.2017.075.
(41) Boyle, M. J.; Richards, J. S.; Gilson, P. R.; Chai, W.; Beeson, J. G. Interactions with heparin-like molecules during erythrocyte invasion by Plasmodium falciparum merozoites. *Blood* **2010**, *115*, 4559−4568.
(42) Saini, E.; Zeeshan, M.; Brady, D.; et al. Photosensitized INA-Labelled protein 1 (PhIL1) is novel component of the inner membrane complex and is required for Plasmodium parasite development. *Sci. Rep.* **2017**, *7*, No. 15577, DOI: 10.1038/s41598-017-15781-z.
(43) Toenhake, C. G.; Fraschka, S. K.; Vijayabaskar, M. S.; et al. Chromatin Accessibility-Based Characterization of the Gene Regulatory Network Underlying Plasmodium falciparum Blood-Stage Development. *Cell Host Microbe* **2018**, *23*, 557−569.e9, DOI: 10.1016/j.chom.2018.03.007.
(44) Singh, G. P. Conservation of gene essentiality in Apicomplexa and its application for prioritization of anti-malarial drug targets. *F1000Research* **2017**, *6*, No. 23, DOI: 10.12688/f1000research.10559.1.
(45) Salinger, D. H.; Nedelman, J. R.; Mendel, C.; Spigelman, M.; Hermann, D. J. Daily Dosing for Bedaquiline in Patients with Tuberculosis. *Antimicrob. Agents Chemother.* **2019**, *63*, No. e00463-19, DOI: 10.1128/AAC.00463-19.
(46) van Heeswijk, R. P. G.; Dannemann, B.; Hoetelmans, R. M. W. Bedaquiline: A review of human pharmacokinetics and drug-drug interactions. *J. Antimicrob. Chemother.* **2014**, *69*, 2310−2318.
(47) Irwin, S. M.; Prideaux, B.; Lyon, E. R.; et al. Bedaquiline and Pyrazinamide Treatment Responses Are Affected by Pulmonary Lesion Heterogeneity in Mycobacterium tuberculosis Infected C3HeB/FeJ Mice. *ACS Infect. Dis.* **2016**, *2*, 251−267.
(48) Carvalho, L. J. M.; Daniel-Ribeiro, C. T.; Goto, H. Malaria vaccine: candidate antigens, mechanisms, constraints and prospects. *Scand. J. Immunol.* **2002**, *56*, 327−343.
(49) Chan, J. A.; Fowkes, F. J. I.; Beeson, J. G. Surface antigens of Plasmodium falciparum-infected erythrocytes as immune targets and malaria vaccine candidates. *Cell. Mol. Life Sci.* **2014**, *71*, 3633−3657.
(50) Chan, J. A.; Howell, K. B.; Reiling, L.; et al. Targets of antibodies against Plasmodium falciparum-infected erythrocytes in malaria immunity. *J. Clin. Invest.* **2012**, *122*, 3227−3238.
(51) Patarroyo, M. E.; Alba, M. P.; Rojas-Luna, R.; Bermudez, A.; Aza-Conde, J. Functionally relevant proteins in *Plasmodium falciparum* host cell invasion. *Immunotherapy* **2017**, *9*, 131−155, DOI: 10.2217/imt-2016-0091.
(52) Frénal, K.; Polonais, V.; Marq, J.-P.; et al. Functional dissection of the apicomplexan glideosome molecular architecture. *Cell Host Microbe* **2010**, *8*, 343−357, DOI: 10.1016/j.chom.2010.09.002.
(53) Dans, M. G.; Weiss, G. E.; Wilson, D. W.; et al. Screening the Medicines for Malaria Venture Pathogen Box for invasion and egress inhibitors of the blood stage of Plasmodium falciparum reveals several inhibitory compounds. *Int. J. Parasitol.* **2020**, *50*, 235−252.
(54) Biendl, S.; Häberli, C.; Keiser, J. Discovery of novel antischistosomal scaffolds from the open access Pandemic Response Box. *Expert Rev. Anti-Infect. Ther.* **2022**, *20*, 621−629, DOI: 10.1080/14787210.2022.1990042.
(55) Samby, K.; Besson, D.; Dutta, A.; et al. The Pandemic Response Box—Accelerating Drug Discovery Efforts after Disease Outbreaks. *ACS Infect. Dis.* **2022**, *8*, 713−720, DOI: 10.1021/acsinfecdis.1c00527.
(56) Van Voorhis, W. C.; Adams, J. H.; Adelfio, R.; et al. Open Source Drug Discovery with the Malaria Box Compound Collection for Neglected Diseases and Beyond. *PLoS Pathog.* **2016**, *12*, No. e1005763.
(57) Samby, K.; Willis, P. A.; Burrows, J. N.; Laleu, B.; Webborn, P. J. H. Actives from MMV Open Access Boxes? A suggested way forward. *PLoS Pathog.* **2021**, *17*, No. e1009384.
(58) Veale, C. G. L. Unpacking the Pathogen Box—An Open Source Tool for Fighting Neglected Tropical Disease. *ChemMedChem.* **2019**, *14*, 386−453.
(59) Allen, A. R.; Macphail, R. C. Bitertanol, A triazole fungicide, increases operant responding but not motor activity. *Neurotoxicol. Teratol.* **1993**, *15*, 237−242.
(60) MacKeigan, J. P.; Krueger, D. A. Differentiating the mTOR inhibitors everolimus and sirolimus in the treatment of tuberous sclerosis complex. *Neuro-Oncol.* **2015**, *17*, 1550−1559.
(61) Lamb, Y. N. Rosuvastatin/Ezetimibe: A Review in Hypercholesterolemia. *Am. J. Cardiovasc. Drugs* **2020**, *20*, 381−392.
(62) Strath, M.; Scott-Finnigan, T.; Gardner, M.; Williamson, D.; Wilson, I. Antimalarial activity of rifampicin in vitro and in rodent models. *Trans. R. Soc. Trop. Med. Hyg.* **1993**, *87*, 211−216, DOI: 10.1016/0035-9203(93)90497-E.
(63) Zaw, M. T.; Emran, N. A.; Lin, Z. Mutations inside rifampicin-resistance determining region of rpoB gene associated with rifampicin-resistance in Mycobacterium tuberculosis. *J. Infect. Public Health* **2018**, *11*, 605−610.
(64) Miller, W. A., III; Teye, J.; Achieng, A. O.; et al. Antimalarials: Review of Plasmepsins as Drug Targets and HIV Protease Inhibitors Interactions. *Curr. Top. Med. Chem.* **2019**, *18*, 2022−2028, DOI: 10.2174/1568026619666181130133548.
(65) Marín-Menéndez, A.; Bell, A. Overexpression, purification and assessment of cyclosporin binding of a family of cyclophilins and cyclophilin-like proteins of the human malarial parasite Plasmodium falciparum. *Protein Expr. Purif.* **2011**, *78*, 225−234.
(66) Tiwari, S.; Sharma, N.; Sharma, G. P.; Mishra, N. Redox interactome in malaria parasite Plasmodium falciparum. *Parasitol. Res.* **2021**, *120*, 423−434.
(67) Dousti, M.; Manzano-Román, R.; Rashidi, S.; et al. A proteomic glimpse into the effect of antimalarial drugs on Plasmodium falciparum proteome towards highlighting possible therapeutic targets. *Pathog. Dis.* **2021**, *79*, No. ftaa071.
(68) Hards, K.; Robson, J. R.; Berney, M.; et al. Bactericidal mode of action of bedaquiline. *J. Antimicrob. Chemother.* **2015**, *70*, 2028−2037.
(69) Rathore, S.; Datta, G.; Kaur, I.; Malhotra, P.; Mohmmed, A. Disruption of cellular homeostasis induces organelle stress and triggers apoptosis like cell-death pathways in malaria parasite. *Cell Death Dis.* **2015**, *6*, e1803.
(70) Jortzik, E.; Becker, K. Thioredoxin and glutathione systems in Plasmodium falciparum. *Int. J. Med. Microbiol.* **2012**, *302*, 187−194.
(71) Pontali, E.; Sotgiu, G.; D'Ambrosio, L.; Centis, R.; Migliori, G. B. Bedaquiline and multidrug-resistant tuberculosis: A systematic and critical analysis of the evidence. *Eur. Respir. J.* **2016**, *47*, 394−402.
(72) Ross, B. N.; Myers, J. N.; Muruato, L. A.; Tapia, D.; Torres, A. G. Evaluating New Compounds to Treat Burkholderia pseudomallei Infections. *Front. Cell. Infect. Microbiol.* **2018**, *8*, No. 210, DOI: 10.3389/fcimb.2018.00210.
(73) Mayer, F. L.; Kronstad, J. W. Discovery of a Novel Antifungal Agent in the Pathogen Box. *mSphere* **2017**, *2*, No. e00120-17, DOI: 10.1128/mSphere.00120-17.
(74) Madhavi Sastry, G.; Adzhigirey, M.; Day, T.; Annabhimoju, R.; Sherman, W. Protein and ligand preparation: Parameters, protocols, and influence on virtual screening enrichments. *J. Comput. Aided Mol. Des.* **2013**, *27*, 221−234.
(75) Friesner, R. A.; Murphy, R. B.; Repasky, M. P.; et al. Extra precision glide: Docking and scoring incorporating a model of hydrophobic enclosure for protein-ligand complexes. *J. Med. Chem.* **2006**, *49*, 6177−6196.
(76) Lyne, P. D.; Lamb, M. L.; Saeh, J. C. Accurate prediction of the relative potencies of members of a series of kinase inhibitors using molecular docking and MM-GBSA scoring. *J. Med. Chem.* **2006**, *49*, 4805−4808.
(77) Bowers, K. J.; Chow, D. E.; Xu, H.et al. In *Scalable Algorithms for Molecular Dynamics Simulations on Commodity Clusters*, Proceedings of the 2006 ACM/IEEE Conference on Supercomputing; IEEE, 2007.
(78) Kumar, I.; Gupta, S. S.; Kumar, R.; et al. Photocatalytic Unsymmetrical Coupling of 2-Substituted Quinolines: Synthesis and

Evaluation of the Antiplasmodial Potential of β-Norbenzomorphan Frameworks. *ACS Sustainable Chem. Eng.* **2020**, *8*, 12902−12910, DOI: 10.1021/acssuschemeng.0c03415.

(79) Huynh, K.; Partch, C. L. Analysis of protein stability and ligand interactions by thermal shift assay. *Curr. Protoc. Protein Sci.* **2015**, *79*, 28.9.1−28.9.14.

(80) Trager, W.; Jensen, J. B. Human malaria parasites in continuous culture. *Science* **1976**, *193*, 673−675.

(81) Witkowski, B.; Amaratunga, C.; Khim, N.; et al. Novel phenotypic assays for the detection of artemisinin-resistant Plasmodium falciparum malaria in Cambodia: in-vitro and ex-vivo drug-response studies. *Lancet Infect. Dis.* **2013**, *13*, 1043−1049.

(82) Thapar, M. M.; Gupta, S.; Spindler, C.; Wernsdorfer, W. H.; Björkman, A. Pharmacodynamic interactions among atovaquone, proguanil and cycloguanil against Plasmodium falciparum in vitro. *Trans. R. Soc. Trop. Med. Hyg.* **2003**, *97*, 331−337.

(83) Meletiadis, J.; Pournaras, S.; Roilides, E.; Walsh, T. J. Defining fractional inhibitory concentration index cutoffs for additive interactions based on self-drug additive combinations, Monte Carlo simulation analysis, and in vitro-in vivo correlation data for antifungal drug combinations against Aspergillus fumi. *Antimicrob. Agents Chemother.* **2010**, *54*, 602−609.

https://doi.org/10.1021/acsomega.3c05323
ACS Omega 2023, 8, 38506−38523